Microbiological Research 277 (2023) 127507

Contents lists available at ScienceDirect

Microbiological Research

journal homepage: www.elsevier.com/locate/micres

Degradation of polypropylene by fungi *Coniochaeta hoffmannii* and *Pleurostoma richardsiae*

Rachel Porter [a,1], Anja Černoša [b,1], Paola Fernández-Sanmartín [c], Antonio Martínez Cortizas [c], Elisabet Aranda [d], Yonglun Luo [e], Polona Zalar [b], Matejka Podlogar [f], Nina Gunde-Cimerman [b], Cene Gostinčar [b,*]

[a] *Biophysics Program, Stanford University School of Medicine, Stanford, CA, USA*
[b] *University of Ljubljana, Biotechnical Faculty, Department of Biology, Jamnikarjeva 101, Ljubljana, Slovenia*
[c] *CRETUS, EcoPast Research Group (GI-1553), Departamento de Edafoloxía e Química Agrícola, Faculty of Biology, Universidade de Santiago de Compostela, Campus Vida, 15782 Santiago de Compostela, Spain*
[d] *University of Granada, Institute of Water Research, Environmental Microbiology Group, Ramón y Cajal n4, 18071 Granada, Spain*
[e] *Lars Bolund Institute of Regenerative Medicine, Qingdao-Europe Advanced Institute for Life Sciences, BGI-Qingdao, Qingdao 266555, China*
[f] *Department for Nanostructured Materials, Jožef Stefan Institute, Jamova cesta 39, Ljubljana, Slovenia*

A R T I C L E I N F O

Keywords:
Biodegradation
Plastic
Hydrocarbons
Spectroscopy
Fungi

A B S T R A C T

The urgent need for better disposal and recycling of plastics has motivated a search for microbes with the ability to degrade synthetic polymers. While microbes capable of metabolizing polyurethane and polyethylene terephthalate have been discovered and even leveraged in enzymatic recycling approaches, microbial degradation of additive-free polypropylene (PP) remains elusive. Here we report the isolation and characterization of two fungal strains with the potential to degrade pure PP. Twenty-seven fungal strains, many isolated from hydrocarbon contaminated sites, were screened for degradation of commercially used textile plastic. Of the candidate strains, two identified as *Coniochaeta hoffmannii* and *Pleurostoma richardsiae* were found to colonize the plastic fibers using scanning electron microscopy (SEM). Further experiments probing degradation of pure PP films were performed using *C. hoffmannii* and *P. richardsiae* and analyzed using SEM, Raman spectroscopy and Fourier transform infrared spectroscopy with attenuated total reflectance (FTIR-ATR). The results showed that the selected fungi were active against pure PP, with distinct differences in the bonds targeted and the degree to which each was altered. Whole genome and transcriptome sequencing was conducted for both strains and the abundance of carbohydrate active enzymes, GC content, and codon usage bias were analyzed in predicted proteomes for each. Enzymatic assays were conducted to assess each strain's ability to degrade naturally occurring compounds as well as synthetic polymers. These investigations revealed potential adaptations to hydrocarbon-rich environments and provide a foundation for further investigation of PP degrading activity in *C. hoffmannii* and *P. richardsiae*.

1. Introduction

Well over 9 billion tons of plastic have been generated since mass production began in the 1950 s, and roughly 75% of this has been consigned to landfills or the natural environment (Geyer, 2020; Geyer et al., 2017). Plastic products require decades or centuries to degrade, and even then, they break down into micro- and nano-plastics. These tiny particles are pervasive in marine environments around the globe and are nearly impossible to recover, posing threats to both human and environmental health (Barnes et al., 2009; Waring et al., 2018; Yee et al., 2021). As the current alternatives to plastic accumulation are carbon-intensive incineration and low-efficiency recycling processes, environmentally and economically sound alternatives are urgently needed to surmount the rising tide of plastic refuse. Recently, strides toward this goal have been made through enzymatic recycling approaches, such as those leveraged by (Tournier et al., 2020). Using an

* Corresponding author.
E-mail address: Cene.Gostincar@bf.uni-lj.si (C. Gostinčar).
[1] Contributed equally to this work as first authors.

https://doi.org/10.1016/j.micres.2023.127507
Received 2 August 2023; Received in revised form 11 September 2023; Accepted 21 September 2023
Available online 27 September 2023

engineered cutinase enzyme, originally discovered in a metagenomic screen of compost isolates, the plastic polyethylene terephthalate (PET) can be efficiently converted into monomers suitable for the synthesis of virgin PET, establishing a viable circular economy for this polymer (Sulaiman et al., 2012; Tournier et al., 2020). This success demonstrates enzymatic recycling processes are viable solutions for plastic waste management, but efficient enzymes are needed to leverage similar approaches against other polymers such as high- and low-density polyethylene (HDPE, LDPE), polyvinyl chloride (PVC), and polypropylene (PP).

In recent years, PP has ranked as the most-used plastic, accounting for 16% of global usage. More PP has been lost to the environment than any other plastic, but the search for PP-degrading enzymes lags behind that for other polymers (Danso et al., 2019; Ryberg et al., 2018). While several studies have reported microbial degradation of PP, many used additive-containing substrates, included UV-treatment steps, or relied solely on weight-based assays, so it is unclear whether the apparent degradation can be wholly ascribed to turnover of pure PP by the microbes of interests (Auta et al., 2018; Cacciari et al., 1993; Oliya et al., 2020; Yang et al., 2021). Pure PP degradation has been demonstrated by bacteria including *Stenotrophomonas panacihumi, Bacillus* sp., and *Rhodococcus* sp., but not in any fungus to the best of our knowledge (Auta et al., 2018; Jeon and Kim, 2016). To address this gap, we screened fungal isolates from hydrocarbon-contaminated environments for activity against synthetic textile fibers.

We focused this screen on fungi based on their broad enzymatic capacities and specialized ability to colonize hydrophobic surfaces. To mineralize complex compounds including cellulose, hemicellulose, and lignin, fungi have evolved complex and often unique enzymatic pathways. Fungal proteomes include an abundance of carbohydrate active enzymes (CAZymes), many of which are secreted to facilitate decomposition of large substrates into smaller byproducts, which can then be imported into the cell for further metabolism. Extracellular activities conferred by the secretome are likely integral for metabolism of high molecular weight polymers. In addition, CAZymes are often highly promiscuous and can thus act against a range of substrates (Pallister et al., 2020). This intrinsic flexibility facilitates adaptation to new substrates, potentially including xenobiotic substances such as plastics (Leveson-Gower et al., 2019). Filamentous fungi also feature a diversity of cytochrome P450 enzymes that is unequalled in other kingdoms, enabling transformation of a range of natural and synthetic substrates (Bezalel et al., 1997; Nelson, 2018; Teramoto et al., 2004). The immense enzymatic capabilities of filamentous fungi have been leveraged both for live-culture bioremediation and enzyme engineering strategies (Asemoloye et al., 2021; Kamali and Khodaparast, 2015). In addition to this arsenal of enzymes, filamentous fungi synthesize and secrete surface-active proteins known as hydrophobins, which facilitate adhesion to hydrophobic surfaces (Wessels et al., 1991). These proteins could play a role in colonization of hydrocarbon rich environments, and have even been shown to enhance enzymatic degradation of PET (Puspitasari et al., 2021).

Together, these features establish fungi as excellent candidates for degradation of synthetic polymers and in fact, numerous fungal species potentially active against polyester polyurethane (PPU), HDPE, LDPE, and PVC have already been identified (Ali et al., 2014; Ojha et al., 2017; Russell et al., 2011). While forays into PP-degrading fungi have been made, further research utilizing additive-free PP is needed. In hopes of addressing this gap, fungi were isolated from a range of hydrocarbon-contaminated environments and screened for activity against synthetic polymers. Of the isolates screened, two strains identified as *Coniochaeta hoffmannii* and *Pleurostoma richardsiae* demonstrated activity against a PP textile and pure PP film. Little information was available on these species beyond their classification as wood rot fungi (Lawrence et al., 2021; Leonhardt et al., 2018). To provide further characterization of these strains and potentially elucidate adaptations to hydrocarbon rich environments, we conducted whole genome sequencing. The genomes and predicted proteomes were then analyzed and compared with related strains, and enzyme assays were conducted to characterize biochemical activities. Our results establish *C. hoffmannii* and *P. richardsiae* as candidates for PP biodegradation and lay the foundation for further exploration of their PP degradation potential.

2. Materials and Methods

2.1. Isolation of fungi

Fungi were isolated from hydrocarbon-contaminated environments, namely from cars (inlets of five car reservoirs), surfaces contaminated with gasoline or diesel fuel (floors contaminated with a mixture of oil, gasoline and water sampled at three car repair shops), water from a shaft inside one car workshop, and gasoline stations (one handle from fuel lines, gasoline-contaminated floors at five stations). Samples were collected with cotton swabs and dabbed onto various antibiotic-containing agar media (malt extract agar with chloramphenicol (MEA Ch); Sabouraud glucose agar with penicillin/streptomycin (SabG pen/strep), and Dichloran Rose Bengal Chloramphenicol agar (DRBC)). The media were incubated at 15 °C, 20 °C, 25 °C, or 37 °C. For isolation of fungi from oil and water mixtures, the flotation method as described in (Satow et al., 2008) was used. The obtained mineral oil/water interface was spread onto SabG or DRBC and incubated at 20 °C or 37 °C. Pure cultures were obtained from colonies and deposited in the Culture Collection Ex (part of Infrastructural Centre Mycosmo, MRIC UL, Department of Biology, Biotechnical Faculty, University of Ljubljana, Slovenia).

2.2. Identification of fungi

Fungi were identified using large subunit (LSU) rDNA domains D1 and D2 26 S or internal transcribed spacer (ITS) rDNA sequences. Genomic DNA of the yeast isolates was extracted by the PrepMan Ultra reagent (Applied Biosystems) according to the manufacturer instructions. DNA of filamentous fungal cultures was extracted as described by (Van Den Ende and De Hoog, 1999). LSU rDNA including D1 and D2 domains and the ITS sequences including the 5.8 S rDNA were amplified and sequenced with the primer sets NL1/NL4 (Kurtzman and Robnett, 1997), and ITS1/ITS4 (White et al., 1990), respectively.

2.3. Initial screening

Strains for the initial screening were obtained from the Culture Collection Ex of Infrastructural Centre Mycosmo (MRIC UL, Department of Biology, Biotechnical Faculty, University of Ljubljana, Slovenia) (Supplementary Table 1). Strains were maintained on malt extract agar (MEA) consisting of 2% malt extract (Biolife, Italy), 0.1% peptone (Merck, Germany), 2% glucose (Kemika, Croatia), and 2% agar (Formedium, UK) in deionized water.

To screen for potential polymer degradation activity, a commercially available PP textile was cut into 1 cm^2 pieces and then sterilized in 96% ethanol for 15 min. After sterilization, the remaining ethanol was removed, and the textiles were dried in a incubation chamber at 37 °C until dry. Sterile textiles were placed in tubes containing 10 mL of liquid M9 medium (pH 7.4), prepared according to Harwood and Cutting (Harwood and Cutting, 1990) using twice distilled (Mili-Q) water, without glucose or other carbon sources.

For yeast strains, cell suspensions were prepared in sterile saline to $OD_{600} = 1.0$, and 400 μL were used to inoculate the tubes containing M9 medium and textile strips. The filamentous strains were inoculated using 4 mm mycelial plugs from an actively growing colony. Two replicates for each strain were prepared, along with two control tubes: one containing only the M9 medium without the textile or the inoculum, and the other contained M9 medium with textile but without the inoculum. The tubes were incubated at 24 °C. After incubation for two and six months,

growth was assessed by adding aniline blue in lactic acid to a few fibers on glass slide and imaging the fungal growth using light microscopy (Olympus BX51, Olympus Microscopy). Promising candidates were further analyzed using chemical fixation followed by scanning electron microscopy (SEM) (Jeol JSM-7600 F, Jeol Ins., Japan), as described below.

2.4. Polymer Degradation Activities

2.4.1. Degradation of PP films

To avoid misleading results due to ambiguous plastic composition and to facilitate spectroscopy measurements, the selected fungi were then cultivated on pure polymer PP films (thickness of 0.012 mm; GoodFellow, United Kingdom). PP films were cut into 1 cm^2 pieces and then sterilized in 96% ethanol for 15 min. After sterilization, the remaining ethanol was removed, and the films were dried at 37 °C.

The PP film pieces were placed on M9 medium without any carbon source, and the strains were inoculated with 4 mm mycelial plugs on the center of the PP films. Three replicates were prepared for each strain. As control PP film pieces were placed on M9 medium without any carbon source and without inoculation. Plates were incubated at 24 °C for two months.

2.4.2. Scanning electron microscopy

Detailed imaging of the contact between fungi and plastic samples was performed by scanning electron microscopy (SEM, Jeol JSM-7600 F, Jeol Ins., Japan). To chemically fix samples for imaging, cultured plastic textile pieces were taken from the growth media and stored in a solution of glutaraldehyde ($C_5H_8O_2$, 25% aqueous solution, Sigma-Aldrich, St. Louis, MO, USA) and sodium cacodylate trihydrate ($C_2H_6AsNaO_2{\cdot}3\,H_2O$, ≥98%, Sigma-Aldrich) at 4 °C for 24 h. The samples were then washed three times in 0.1 M sodium cacodylate buffer with pH 8.28, for 20 min each. This was followed by one minute rinsing in Mili-Q water and dehydration with increasing concentrations of absolute ethanol (C_2H_5OH, absolute for analysis EMSURE® ACS, ISO, Reag. Ph Eur, Merck), namely 25%, 50%, 75%, 95% and 99.9% for 10-minute intervals. The last step of fixation was rinsing in hexamethyldisilazane (HMDS, Sigma-Aldrich) for 5 min. Finally, the samples were air-dried in a dust-free chamber and coated with carbon (Precision Etching Coating System, PECS, Model 682, Gatan, Pleasanton, CA, USA) before detailed imaging of fungi-plastic contact by SEM. For the general assessment of fungal growth on plastic films, the chemical fixation was not needed. Drying samples and coating them with carbon or gold to avoid charging effect in SEM was unnecessary, as environmental SEM (ESEM, Quanta 650, Thermo Fisher Scientific, Waltham, Massachusetts, USA) enables low vacuum imaging. Thus, film samples were collected and directly placed on the SEM holder for analysis.

2.4.3. Raman spectroscopy

In addition to SEM, Raman spectroscopy was used to assess chemical changes to plastic films following fungal colonization. Using a confocal Raman spectrometer (Integra Spectra I, NT-MDT Co., Russia), a blue wavelength laser with 488 nm was focused on the plastic sample surface at positions both with and without fungi, in Raman shift range from 200 to 3000 cm^{-1}. Spectra were acquired upon 10 s of exposure with 5 times accumulation. Three spectra were taken to get the average at each position. For every spectrum, baseline absorbance was subtracted and treated samples were normalized to untreated controls to determine relative changes in different bond vibrations.

2.4.4. Fourier-transform infrared spectroscopy

After the incubation the film samples were analyzed using attenuated total reflectance Fourier-transform infrared spectroscopy (FTIR-ATR) with an Agilent Cary 630 spectrometer, equipped with a single reflection diamond crystal, previously described by (Fernández-Sanmartín et al., 2023). FTIR-ATR spectra were acquired at 4 cm^{-1} resolution in the mid-infrared (MIR) region (4000–400 cm^{-1}), by averaging 200 scans. As controls, the films without the treatment were used. Twenty-five measurements were performed on each plastic film arranged on a grid of approximately 1.5 × 1 cm. Given the size of the diamond crystal of the MIR equipment (3 ×1 mm), the measured area was about 50% of the surface of the screened plastic surface.

The R package 'andurinha' (Alvarez Fernandez and Matrinez Cortizas, 2022; R Development Core Team, 2020) was used to obtain standardized spectra, second derivative spectra, average spectrum and standard deviation spectrum. Using the same package, locations of the relevant bands and standardized absorbances for each band and sample were identified. Assignment of bands was based on existing literature (Nishikida & Coates 2003; Selling & Campos 2003; Chércoles et al., 2009; Kang et al., 2013; Chibani et al., 2014; Jung et al., 2018; Peets et al., 2019; Gall et al., 2021; Okubo et al., 2022).

To trace polypropylene (PP) degradation, we performed principal components analysis (PCA) on 30 relevant MIR bands extracted using 'andurinha'. The analysis was done on the correlation matrix and with varimax rotation. ANOVA analysis was applied to the principal components' scores to assess for significant differences between the untreated PP (PP untr) plastic and the samples treated with the fungi (PP EXF-13287 and PP EXF-13308). ANOVA was also used to test for significant decreases in relative absorbance (RA) for bands with high loadings in those principal components that showed significant differences between the treated and untreated plastics. The percent relative absorbance (A_r) was calculated according to the following formula:

$$A_r = \frac{A_f - A_i}{A_i} \times 100 \tag{1}$$

where A_i is the initial absorbance before incubation and A_f is the final absorbance following incubation.

$$CV = \frac{s}{\mu} \times 100 \tag{2}$$

The coefficient of variation (CV, described in Eq.2., where s is the standard deviation and μ is the mean) of the absorbances for the representative bands of polypropylene before and after incubation was also calculated in triplicate. Bands with CV ≥ 25 were discarded, to avoid bias due to spectral heterogeneity.

2.5. Characterization of Enzymatic Activities

Enzymatic activities were probed using plate assays for amylase, beta-glucosidase, cellulase, xylanase, pectinase, chitinase, laccase, tannase, esterase, feruloyl esterase, gelatinase, caseinase, and urease activities. Strains were cultivated on YNB (0.17% yeast nitrogen base (Qbiogene, Carlsbad, CA, USA) with 0.5% ammonium sulfate (Sigma-Aldrich) in deionized water at pH 7) plates made with 2% agar (Formedium, Hunstanton, UK). Four mm plugs from regions of confluent growth were used to inoculate plate assays. All assays were conducted in triplicate, with the exceptions of the pectinase assay (n = 2) and the laccase assay (n = 9). For amylase, pectinase, cellulase, and caseinase assays, the enzymatic indices were tabulated according to Eq. 3 and all others were interpreted as positive or negative. As some colonies and clearance zones were irregularly shaped, the normalized radii were calculated by finding the area (A) of the entire colony or clearance zone in Fiji (Schindelin et al., 2012), and using Eq. 4 to find the effective radius (r).

$$EI = \frac{radius\ \ of\ \ colony\ \ and\ \ clearance\ \ zone}{radius\ \ of\ \ colony\ \ only} \tag{3}$$

$$r = \left(\frac{A}{\pi}\right)^{1/2} \tag{4}$$

Significant differences between EI values were identified using a

Student's T-test with ScipPy's statistics package (Virtanen et al., 2020).

To assess amylolytic activity, a modified version of the procedure by (Dodman and Reinke, 1982) was used, as previously described (Zajc et al., 2019). Samples were cultivated on media supplemented with soluble starch for two weeks, then exposed to iodine vapors (Sigma-Aldrich) to reveal clearance zones indicative of amylolytic activity. Beta-glucosidase activity was tested using aesculin agar, as described in (Paterson and Bridge, 1994) and (Zajc et al., 2019). After two weeks of growth, plates were checked for black coloration, which results from reaction of ferric citrate with aesculetin, a byproduct of aesculin degradation. Cellulolytic activity was characterized using an assay described by (Paterson and Bridge, 1994), in which samples are grown on media including 4% carboxymethyl cellulase (Sigma-Aldrich). After two weeks of incubation, plates were stained with 0.3% Congo Red (Merck, Darmstadt, Germany). Zones of clearance indicated degradation of carboxymethyl cellulase and thus a positive result. Xylanolytic activity was measured similarly, using xylan (Sigma-Aldrich) in place of carboxymethyl cellulase (Zajc et al., 2019). Pectinase activity was assessed using media supplemented with apple pectin (Sigma-Aldrich). Following two weeks of incubation, plates were flooded with iodine solution (Sigma-Aldrich) and zones of clearance were interpreted as a positive result and measured (Hankin et al., 1971; Hitha and Girija, 2014; Zajc et al., 2019).

To test chitinase activity, media prepared with colloidal chitin from crab shells and bromocresol purple (Sigma-Aldrich) as described by Zajc et al. (2019) was used. Formation of a purple zone after two weeks of growth indicated chitinase activity. Laccase activity was tested in rich media supplemented with 0.01% guaiacol (Gaur et al., 2018). Following a two-week incubation period, plates were checked for formation of a purple compound, indicative of laccase degradation activity. Tannase activity was assessed by degradation of 1% tannic acid in a mineral medium (Cavalcanti et al., 2017). After incubation for two weeks, the plates were checked for halos around the colonies.

An assay described by (Lelliott and Stead, 1987) was used to check for esterase activity. Samples were cultivated on media supplemented with Tween-80, peptone (Conda Pronadisa, Torrejon de Ardoz, Spain), and bromocresol purple (Sigma-Aldrich) for two weeks, after which plates were checked for purple coloration with a white precipitate surrounding the colony as a positive result. Feruloyl esterase activity was tested using a modification of a previously described assay (Donaghy et al., 1998). Media was made as described before, with addition of 2% ethyl ferulate (Sigma-Aldrich) (10% v/v in dimethylformamide) at the plate-pouring stage. Plates were incubated for two weeks after which zones of clearance indicating feruloyl esterase activity were measured.

Proteolytic activity was investigated using gelatinase and caseinase assays. To assess gelatinase activity, a modified version of the procedure by (Hankin and Anagnostakis, 1975) was used. Plates with 12% gelatin (Sigma-Aldrich), 0.3% beef extract (Beeton Dickinson, Franklin Lakes, NJ, USA), and 0.5% peptone (Merck) were inoculated and cultured for 3 weeks and checked for an indentation, indicating liquefaction of the gelatin, and thus a positive reaction. Caseinase activity was characterized by assessing degradation of casein (Brizzio et al., 2007). Formation of a clear zone around colonies following 2 weeks of incubation was interpreted as a positive result.

Urease activity was probed using an assay described in (Paterson and Bridge, 1994). Media containing 2% urea and bromocresol purple (both Sigma-Aldrich) was inoculated, and urease-positive samples were identified by a change in color from red to purple after two weeks of growth.

2.6. Assimilation of Hydrocarbons

Assimilation of hydrocarbons was determined according to (Satow et al., 2008) and modified by (Zajc et al., 2019). Liquid YNB medium without a carbon source was autoclaved, then supplemented with 0.22 μm filter-sterilized 20% (v/v) mineral oil or 20% (v/v) n-hexadecane (both Sigma-Aldrich) as the sole carbon source. Test tubes were inoculated with a 4 mm diameter mycelial plug from an actively growing colony and incubated at room temperature for one month without shaking. Visible growth was interpreted as a positive result for assimilation of the provided hydrocarbon.

2.7. Sequencing and Assembly

Sequencing for the *C. hoffmannii* (EXF-13287) and *P. richardsiae* (EXF-13308) isolates (henceforth denoted CH01 and PR01, respectively) was conducted as described in (Gostinčar et al., 2018). Briefly, strains were grown in liquid YNB at 24 °C, with shaking. Cells were harvested in mid-exponential phase by centrifuging for 10 min at 5000g, then frozen in liquid nitrogen and stored at −80 °C. Frozen tissues were then ground with mortar and pestle, and DNA and RNA were isolated using the UltraClean Microbial DNA isolation kit (MO BIO Laboratories, USA) and TRI Reagent (Sigma-Aldrich, Germany), respectively, each according to manufacturer instructions.

Genomic DNA and transcriptomic RNA were sequenced by the BGI Europe Genome Center using the DNBSEQ technology. Paired-end 150 bp reads were obtained for genome sequencing, and paired-end 100 bp reads were obtained for non-stranded and polyA-selected RNA sequencing. Raw sequencing reads were trimmed with Sickle 1.33 (Joshi and Fass, 2011) to a minimum Phred score of 30, discarding all reads shorter than 45 bp after quality trimming. The genome-sequencing reads were assembled with SPAdes 3.13.0 (Prjibelski et al., 2020), using the option "–careful" and other parameters left at default values. Gene prediction for each strain was conducted with AUGUSTUS 3.3.2 (Stanke and Morgenstern, 2005) on an assembled genome masked with RepeatMasker 4.0.9 (Smit et al., 2013–2015). The completeness of assembly and annotation was evaluated with searching for Benchmarking Universal Single-Copy Orthologs (BUSCOs) with BUSCO 4.1.1 (Manni et al., 2021) using 'sordariomycetes_odb10′ list of orthologs (Zdobnov et al., 2021) as the benchmark. Transcriptomic data was assembled with Trinity (Grabherr et al., 2011) and transcripts with an expression value of 100 transcripts per million (TPM) or above were used as hints for the gene prediction, together with the fungal component of the OrthoDB, downloaded on 19. 1. 2021 (Kriventseva et al., 2019).

Additionally, the type strain of *C. hoffmannii* (CBS 245.38) was included in bioinformatic and enzymatic analyses. This strain (denoted CH02) was cultured from the holotype of *C. hoffmannii* in Suhr, Switzerland and sequenced by (Leonhardt et al., 2018) (GenBank accession: MG491499). A specimen was obtained from Westerdijk Fungal Biodiversity Institute in Utrecht, Netherlands and used for enzymatic assays alongside our isolates. Gene prediction for CH02 was conducted using transcriptomic data for CH01 as hints. Special care was taken in analysis of the predicted CH02 proteome to ensure the use of data from strain CH01 did not exert undue influence over CH02 predictions. For example, several short introns were predicted in CH02 coding sequences, masking indels which would otherwise cause frameshifts relative to CH01, thus greatly decreasing similarity in predicted protein sequences. When comparing orthologs between CH01 and CH02, manual inspection of multiple sequence alignments (MSAs) generated by Clustal Omega (Sievers et al., 2011) was used to avoid such biases.

2.8. Gene prediction and classification

The dbCAN2 server (Zhang et al., 2018) was used to run DIAMOND (Buchfink et al., 2021), HMMer (Eddy, 2011), Hotpep (Busk et al., 2017), and SignalP (Almagro Armenteros et al., 2019) to identify CAZy motifs and peptide signal sequences in the predicted proteomes for CH01, CH02, and PR01. CAZy classifications were considered significant when made by at least two of the three programs. To identify proteins unique to CH01 or CH02, orthologs were paired using BLAST (Altschul et al., 1990). Unmatched proteins were considered 'unique' to a strain if

in the other strain, the corresponding coding sequence was missing or severely mutated. Functional predictions for unique proteins were made using three or more iterations of PSIBLAST (Altschul et al., 1997) as needed. CAZyme annotations for related *Coniochaeta* strains (C. sp.: 2T2.1 and PMI_546; *C. ligniaria*: R110.5, CBS 111746, and NRRL30616) were obtained from JGI MycoCosm (Grigoriev et al., 2012; Nordberg et al., 2014). Assignment of CAZyme classes to putative substrates followed those previously described by Sista Kameshwar and Qin, shown in Table 1 (Sista Kameshwar and Qin, 2018).

2.9. Assessment of Codon Usage Bias and GC Content

Overall codon usage frequencies and position-specific GC contents for CH01, CH02, and PR01 were calculated using EMBOSS CUSP on all coding sequences, regardless of expression, for comparison with codon usage frequencies in the coding sequences of *C. albicans*, *A. nidulans*, *K. lactis*, *N. crassa*, *S. pombe*, and *S. cerevisiae* included in the EMBOSS software (Rice et al., 2000). Species-specific codon preferences for calculation of codon adaptation index (CAI) were determined using CUSP on highly expressed genes, defined as the top 10% of expressed genes based on CH01 and PR01 transcriptomic data. CAI values for individual coding sequences were calculated using these codon preferences in EMBOSS CAI (Sharp and Li, 1987). Overall GC contents and effective number of codons (Nc) values were calculated for individual coding sequences using CodonW software (Peden, 1999).

2.10. Data Analysis and Visualization

Data were processed using Python (Guido Van and Fred, 2009), including the packages SciPy (Virtanen et al., 2020) for statistics, Matplotlib (Hunter, 2007) and seaborn (Waskom, 2021) for visualization, and Scikit-Learn for principal component analysis (Pedregosa et al., 2011). A bootstrapping analysis was conducted to determine the significance of differences in position-specific GC contents between all identified coding sequences and highly expressed coding sequences. Thirty-five random samples containing 10% of all coding sequences were used to find distributions of GC, GC1, GC2, and GC3 values for CH01 and PR01. After verifying that these distributions were approximately Normal, the values obtained for the 10% of coding sequences with the highest expression were compared to the bootstrapped distributions in SciPy to determine the significance of observed differences.

3. Results

3.1. Initial screening

Twenty-two strains, isolated from hydrocarbon (oil and gasoline) contaminated sites, including auto repair shops and gasoline stations, were selected for this study (Supplementary Table 1). The strains were tested for growth on a commercial plastic PP textile. After periods of 17 days and 2 months of cultivation on a commercial plastic PP textile, samples were visualized by light microscopy and SEM for fungal proliferation. Of the 22 isolates screened, *Acremonium sclerotigenum, Coniochaeta hoffmannii,* and *Pleurostoma richardsiae* demonstrated notably more growth on the plastic fibers than other strains (Fig. 1). Fungal growth was observed by light microscopy on individual fibers already after 17 days (Fig. 1**A,B,C**), and was pronounced after 2 months of incubation, especially those inoculated with *Coniochaeta hoffmannii* and *Pleurostoma richardsiae* (Fig. 1**D,E,F**). Fig. 1**G,H,I** show SEM images of surface details of plastic fibers overgrown with *Acremonium sclerotigenum*, *Pleurostoma richardsiae,* and *Coniochaeta hoffmannii* after two months.

Table 1
Assignment of CAZyme classes to putative substrates.

Substrate:	CAZyme Classes:
Lignin	AA1, AA2, AA3, AA4, AA5, AA6, AA8, AA9, AA11, AA12, AA13
Cellulose	GH1, GH2, GH3, GH5, GH6, GH7, GH8, GH9, GH38, GH44, GH45, GH48, GH74
Hemicellulose	GH10, GH11, GH12, GH27, GH31, GH35, GH39, GH43, GH47, GH78, CE1, CE2, CE3, CE4, CE5, CE6, CE7
Pectin	PL3, PL4, PL9, GH28, GH78, GH88, GH95, GH105, GH115, CE8, CE12

(AA = auxiliary activities, CE = carbohydrate esterases, GH = glycoside hydrolases, PL = polysaccharide lyases)

3.2. Pure PP degradation

While these initial findings hinted at polymer degradation activities, the textiles likely contained a complex mixture of additives. To exclude confounding growth of fungi due to additives in the polymers, fungal growth on pure PP film was characterized. Based on their success in the previous textile utilization experiment, we focused on the isolated strains of *Pleurostoma richardsiae* (PR01) and *Coniochaeta hoffmannii* (CH01). SEM, Raman spectroscopy, and Fourier transform infrared spectroscopy with attenuated total reflectance (FTIR-ATR) were used to visualize fungal proliferation and detect changes in chemical bonds along the surface of the films (Figs 2 and 3).

As shown in Fig. 2, *C. hoffmannii* demonstrated a more extensive spread across the film, during the growth period, compared to *P. richardsiae.* Employing confocal Raman spectroscopy at the infested site, notable changes in the polymer structure were observed. Raw spectra of treated polymers exhibited increased noise and reduced peak intensities, as expected due to the diminished polymer structure (Guo et al., 2019; Mei et al., 2022). Upon subtracting the background and normalizing intensities to one of the backbone vibrations, namely C-C stretching with CH bending at 1153 cm^{-1} (Prokhorov et al., 2016), significant changes were observed in normal modes, including pure CH, CH_2 and/or CH_3 kinetics. Notably, *C. hoffmannii* treatment led to a noticeable increase in the relative population of methyl groups and also CH_2 (symmetric and asymmetric stretching seen at 2840–2960 cm^{-1} are increased). In contrast, *P. richardsiae* treatment resulted in a decrease only in the symmetric CH_3 vibration. Furthermore, *P. richardsiae* treatment exhibited a decrease in peak absorption at 401 and 812 cm^{-1}, associated with CH bonds and a decrease at 843 associated with C-CH_3 and CH_2 (de Báez et al., 1995). In contrast, *C. hoffmannii* exposure leads to increase in all the mentioned peaks, suggesting a relative increase of the corresponding bonding. Interestingly, a new broad peak is observed around 1600 cm^{-1} for *P. richardsiae*-treated films, possibly associated with symmetric C=C stretching.

For a more comprehensive and statistically significant analysis, FTIR spectroscopy was employed. Fig. 3 shows the average spectra (A), second derivative spectrum (B), and standard deviation spectra (C) of the untreated and treated with *C. hoffmannii* (PP EXF-13287) and *P. richardsiae* (PP EXF-13308) polypropylene. All 75 individual spectra can be found in supporting material (Fig. 3**G**). Overall high absorbance was found in the 3000–2800 cm^{-1} region, and bands at 1461, 1450 and 1375 cm^{-1}; moderate to low absorbance was also found at 1357, 1167, 997, 973, 900, 841 and 809 cm^{-1}; while low absorbance and poorly defined shoulders were detected at 2721, 1739, 1655, 1545, 1329, 1305, 1293, 1254, 1219, 1152, 1101, 1044, and 939 cm^{-1} (Fig. 3**B**).

The standard deviation spectra (Fig. 3**C**) show that the untreated plastic had the most homogeneous (i.e., lower standard deviation) composition, except for bands at 2950 and 1375 cm^{-1}, the region between 1100 and 950 cm^{-1} that showed relatively large values, and bands at 2866 and 1461–1450 cm^{-1} that showed moderate standard deviation values. Sample PP EXF-13287 showed high to moderate variability for bands at 1950, 2919, 2866, 1461–1450, 1375, 1167, 997, 973, and 841 cm^{-1}, while sample PP EXF-13308 showed large variability at 2950, 2866, 1739, 1655, 1545, and 1375 cm^{-1}, and moderate variability at 1461–1450, 1254, 1219, 997, 973, 841, and 809 cm^{-1}.

In the PCA performed on 30 selected MIR bands, four components

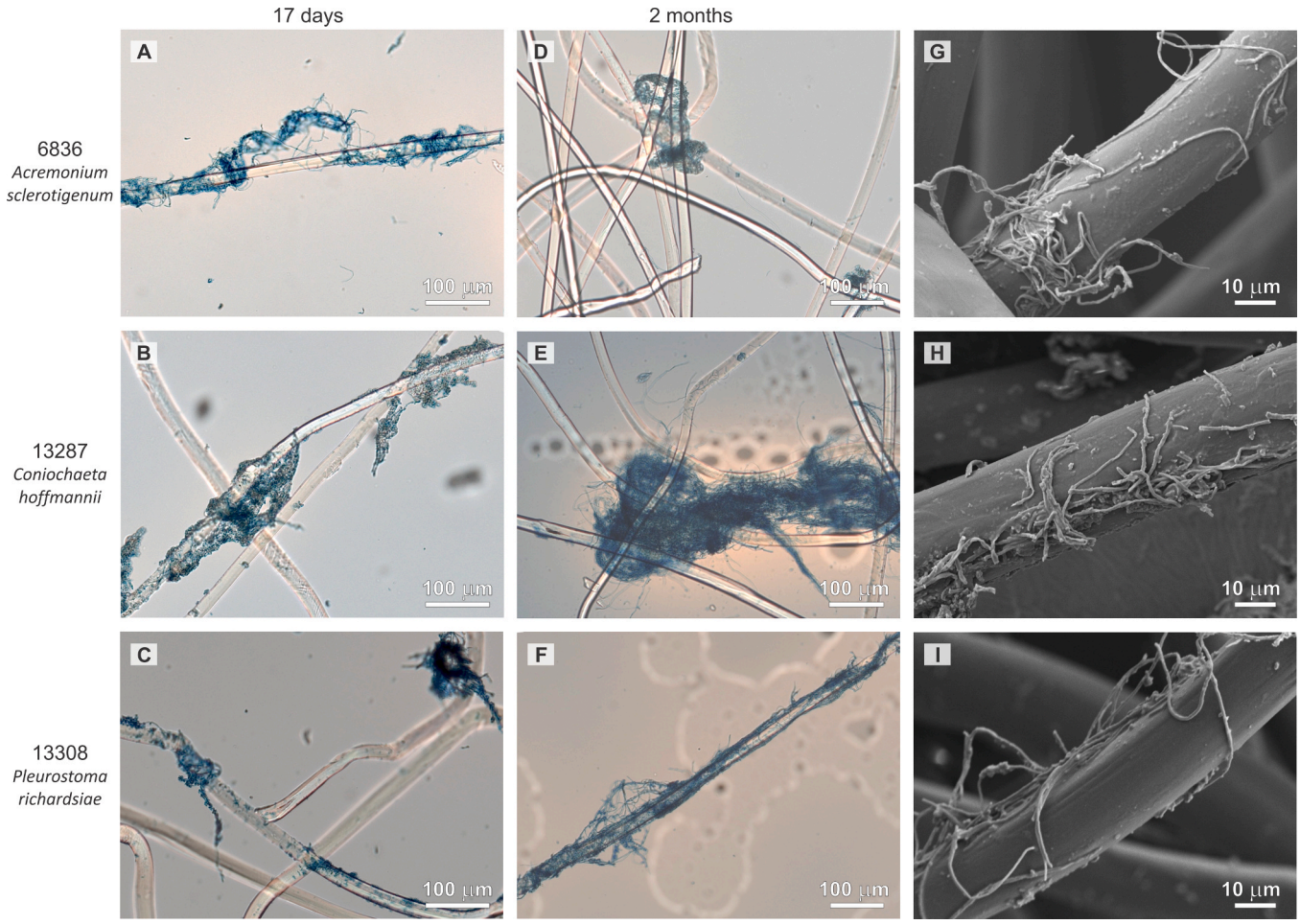

Fig. 1. Filamentous fungi *A. sclerotigenum*, *C. hoffmannii*, and *P. richardsiae* can grow on microplastics. Light microscope images of (A) *A. sclerotigenum*, (B) *C. hoffmannii* and (C) *P. richardsiae* after 17 days, and after two months (D, E, F) of growth on synthetic textile fibers. (G, H, I) Close-up SEM images showing surfaces of synthetic textile fibers overgrown by (G) *A. sclerotigenum*, (H) *C. hoffmannii* and (I) *P. richardsiae* after 2 months of cultivation.

were found to be significant (i.e., eigenvalue > 1). The first component (Cp1, 45.5% of the MIR variance) showed large (>0.7) positive loadings for bands at 2963, 2950, 2838, 1450, 1305, 1167, 1152, 997, 973, and 941 cm^{-1}, and a moderate positive loading for 1256 cm^{-1} (Table 2). Large negative (<−0.7) loadings were obtained for 2866, 1919, 1357, and 1375 cm^{-1}.

The second component (Cp2, 26,9% of total MIR variance) showed large positive loadings for bands at 939, 900, and 809 cm^{-1}, and large negative loadings for bands at 1739, 1655, 1545, 1293, and 1219 cm^{-1} (Table 2). The third (Cp3, 7.4% of total variance) and fourth (Cp4, 4.8% of the total variance) only showed large loadings for bands at 1101 and 1044 cm^{-1}, and 1461 cm^{-1} respectively (Table 2).

ANOVA analysis on the components' scores indicated that Cp1 and Cp2 showed significant differences between the untreated and treated (PP EXF-13287 and PP EXF-13308) polypropylene, while differences for Cp3 and Cp4 were not significant (Supplementary Table 2). Tukey test for homogeneous groups indicated that PP EXF-13287 showed significantly larger Cp1 scores than PP EXF-13308 and untreated PP; however, the latter two did not differ significantly. For Cp2 scores all groups were found to differ significantly (PP untreated < PP EXF-13287 < PP EXF-13308).

The Cp1-Cp2 projection of the samples is depicted in Fig. 3**D**. All measurements done in untreated polypropylene fall in the upper left quadrant, meaning that this condition had larger absorbances for bands with negative loadings in Cp1 (2866, 2919, 1357, and 1375 cm^{-1}) and positive loadings in Cp2 (939, 900, and 809 cm^{-1}). The treated polypropylene departed from the untreated polypropylene and, as already mentioned, also differed from the untreated polypropylene and from each other (Fig. 3**D**). *P. richardsiae* attack resulted in variable decreases in CH_2, CH_3, and C-C vibrations (Table 2); while *C. hoffmannii* attack resulted in moderate decreases of those vibrations, but larger decreases in CH, CH_2, CH_3, C-CH_2, C-CH_3, and C-C vibrations (Table 2). Spatial variability in Cp1 scores in the treated and untreated plastic samples was relatively low, but it was larger for Cp2 scores of PP EXF-13308 (Fig. 3**E**). This suggests that *C. hoffmannii* produced more homogeneous polypropylene degradation than *P. richardsiae*.

ANOVA test also indicated that significant decreases in relative absorbance occurred for 10 out of 13 bands related to polypropylene integrity (Fig. 3**F**). The largest decreases (>10%) were found for bands at 939, 900 and 809 cm^{-1} for both fungi, and for band 1329 cm^{-1} for PP EXF-13287. Significant, moderate decreases (5–10%) were also found for 2919, 2866, 1375, and 1357 cm^{-1}, and low decreases for 2919, 2879, and 1461 cm^{-1} for PP EXF-13287. For PP EXF-13308, although decreases in 2879, 1461, and 1375 cm^{-1} were significant, they were quite low (<3%).

3.3. Sequencing, and assembly

Based on their successful growth on plastic textile fibers and pure PP film, *P. richardsiae* and *C. hoffmannii* (PR01 and CH01, respectively) were selected for further characterization. *P. richardsiae* and *C. hoffmannii* are closely related, both belonging to the subclass *Sordariomycetidae* along with the model species *Neurospora crassa*. Little is known about each of these strains beyond their wood-rot lifestyles and

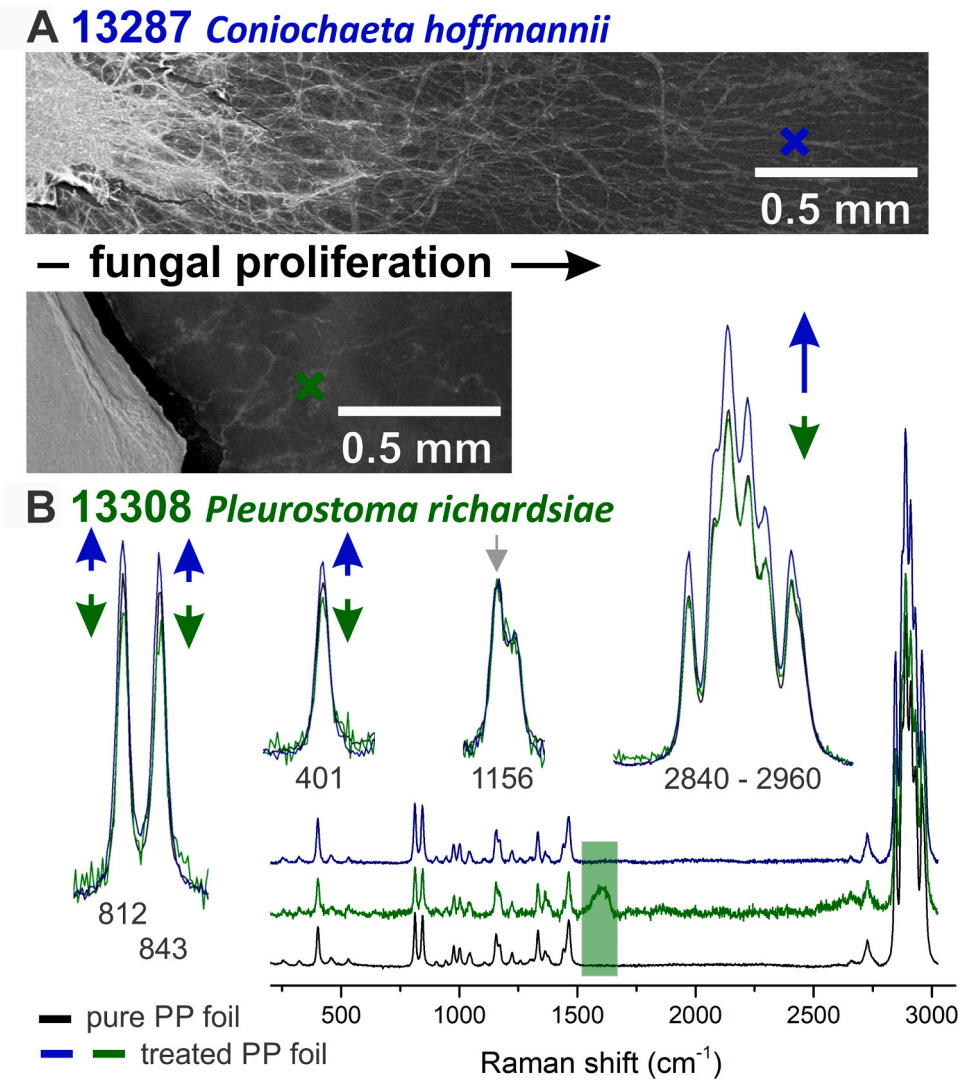

Fig. 2. The selected fungi *C. hoffmannii* and *P. richardsiae* grow on pure polypropylene (PP) film. SEM images show that *C. hoffmannii* (A) spreads across the surface more than *P. richardsiae* (B). Raman spectroscopy reveals PP bond damage due to overgrowth of each fungus on the surface of the film.

initial isolation conditions, so we sought to address this gap, starting with whole genome and transcriptome sequencing. Over 20 mio reads were obtained through sequencing CH01 genomic DNA and over 50 mio reads were obtained for PR01 (in both cases 2 ×150 bp), representing 96 × and 202 × genome coverage, respectively. Transcriptome sequences produced more than 90 mio paired-end 100 bp-long reads for each species.

Genomic data was assembled using SPAdes. The assembled genome of CH01 was 32.69 Mbp long and consisted of 413 contigs with an N50 value of 149,529 bp and 0.96% repetitive DNA. The genome of PR01 was 39.90 Mbp long and contained 341 contigs with an N50 length of 691,216% and 0.78% repetitive DNA. Transcriptomes for each strain were assembled using Trinity. Transcripts with more than 100 transcripts per million (TPM), which totaled 5366 in CH01 and 5078 in PR01, were used as hints for genome prediction. The assembled genomes and transcriptomic data for CH01 and PR01 were then used to direct gene prediction in CH01, PR01, and an additional *C. hoffmannii* strain for which the genome is publicly available, CH02, using AUGUSTUS. A total of 10,418, 10,666, and 12,568 protein coding sequences were predicted for strains CH01, CH02, and PR01, respectively.

Completeness of genome assemblies and annotations for CH01 and PR01 was evaluated by searching for Benchmarking Universal Single-Copy Orthologs (BUSCOs). Of 3817 orthologs universally present in Sordariomycetes, 3750 (98.2%) were found to be complete in CH01 and 3757 (98.4%) in PR01, with additional 36 and 38 genes found as fragmented in each species, leaving only 0.9% and 0.6% genes as missing entirely. The raw reads and the assembled and annotated genomes have been deposited in GenBank and are available under BioProject accession numbers PRJNA854363 (CH01) and PRJNA854364 (PR01).

3.4. Proteome prediction and classification

For the CH01, CH02, and PR01 predicted proteomes, putative carbohydrate active enzymes (CAZymes) and peptide signal sequences were identified using a local installation of the server dbCAN2. A total of 481, 466, and 526 CAZy motifs were identified across 433, 421, and 483 proteins in strains CH01, CH02, and PR01 (Fig. 4). Most proteins feature a single motif, but several include two or even three motifs, thus there are fewer CAZyme proteins than CAZy motifs for each strain (Supplementary Table 3). Compared to five related *Coniochaeta* strains included in the JGI MycoCosm database, CH01 and CH02 have fewer CAZymes, with values of 481 and 466 compared to 642, 654, 656, 696, and 1378, though this difference may be due to methodological differences in their identification.

The distribution of CAZy motifs among the six CAZyme categories (auxiliary activities (AA), carbohydrate binding motifs (CBM),

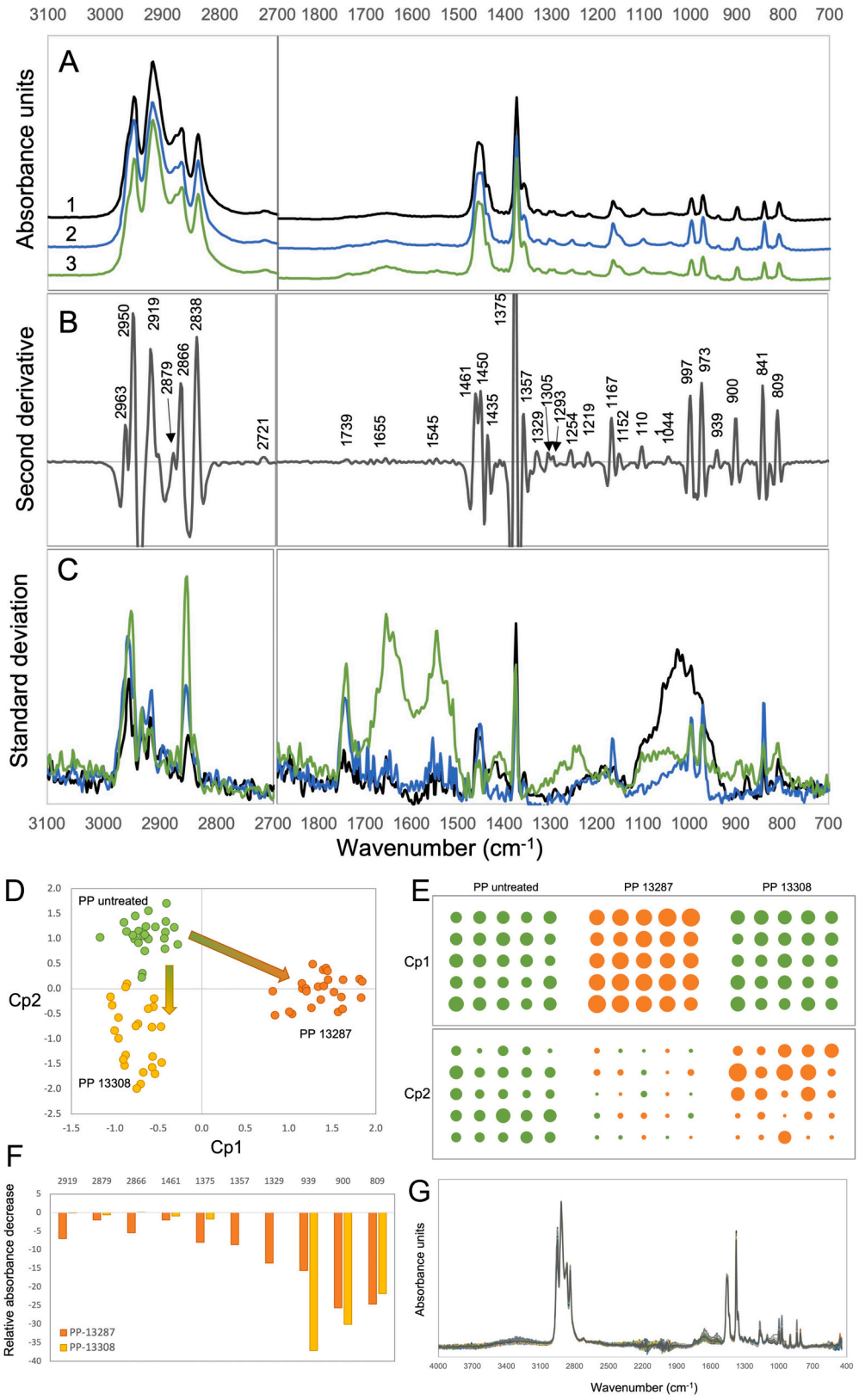

Fig. 3. Fungal colonization with *C. hoffmannii* and *P. richardsiae* differentially alters PP bonds. (A) Average (1. PP untreated – black line, 2. PP EXF-13287 – blue line, 3. PP EXF-13308 – green line) spectra, (B) second derivative spectrum and (C) standard deviation spectra of the polypropylene samples analyzed. (D) Cp1-Cp2 projection of the PCA scores suggesting two degradation pathways. (E) Cp1-Cp2 scores: the size of the circles is proportional to the score value. Green: plastic integrity not affected; orange: plastic integrity affected. (F) Relative decrease in absorbance for CP1 and Cp2 resulting from fungi attack. (G) Whole MIR spectra of the analyzed plastic samples (75 measurements).

Table 2
Results of the PCA performed on the most relevant polypropylene bands. WN: wavenumber; vibrations: bd, bending; rk, rocking; st, stretching; tw, twisting; wg, wagging). References: 1. Nishikida & Coates 2003; 2. Selling & Campos 2003; 3. Chércoles et al., 2009; 4. Fang et al., 2012; 5. Chibani et al., 2014; 6. Jung et al., 2018; 7. Peets et al., 2019; 8. Okubo et al., 2022).

WN	Cp1	Cp2	Cp3	Cp4	Band assignment
1167	**0,98**	-0,01	-0,06	-0,10	CH wg + CH3 rk + C-C st (3, 4, 5, 6)
841	**0,97**	0,17	-0,06	-0,06	CH2 rk + C-CH2 st + C-CH3 st (3, 4, 5, 6)
973	**0,95**	0,25	0,07	0,00	CH3 rk + CH2 rk + CH wg + CH bd + C-C st + C-C rk (3, 4, 5, 6)
997	**0,94**	0,26	0,12	0,01	CH2 rk wg + CH3 rk + CH3 bd + CH bd (3, 4, 5, 6)
2963	**0,94**	0,22	-0,04	-0,14	CH st (7)
1305	**0,88**	-0,32	-0,13	-0,11	CH st (5)
2838	**0,88**	0,34	-0,12	-0,07	CH st + CH2 st (3, 5)
2950	**0,88**	0,38	-0,03	-0,06	CH st + CH2 st (3, 5, 6, 7)
1450	**0,85**	0,23	0,16	0,31	CH2 bd (3, 6)
1152	**0,81**	-0,36	-0,04	-0,21	C-C polymer backbone (3)
1256	**0,62**	-0,61	-0,12	-0,13	CH2 wg + CH bd (5)
2879	**-0,63**	0,52	-0,02	-0,07	CH3 st (3, 4)
1375	**-0,80**	0,34	0,13	0,43	CH3 bd (3, 4, 5, 6)
1357	**-0,88**	-0,02	0,10	0,32	CH bd + CH2 wg (5)
2919	**-0,97**	0,09	0,00	0,11	CH2 st (3, 4, 6)
2866	**-0,98**	0,07	0,03	0,08	CH3 st (3)
900	-0,24	**0,93**	0,03	0,19	CH2 rk - C-C st (3, 5)
939	0,14	**0,90**	0,21	0,19	CH3 rk + C-C sym st (5)
809	-0,41	**0,83**	0,10	0,26	CH2 rk + C-C st (3, 4, 5, 6)
1293	-0,35	**-0,69**	-0,27	0,04	CH2 tw (8)
1219	-0,27	**-0,72**	-0,24	-0,11	CH bd (5)
1739	-0,18	**-0,75**	-0,22	-0,07	C═O (1)
1545	-0,22	**-0,94**	-0,07	0,08	CONH (amido group) (1)
1655	-0,21	**-0,94**	-0,03	0,06	C═O (2)
1101	-0,27	0,16	**0,92**	0,09	C-O ester (2)
1044	0,15	0,25	**0,90**	0,13	benze (phthalate) ring (1)
1461	-0,39	0,26	0,27	**0,82**	CH3 bd (4, 6, 7)

carbohydrate esterases (CE), glycoside hydrolases (GH), glycosyl transferases (GT), and polysaccharide lyases (PL)), is generally conserved between CH01, CH02, and the related *Coniochaeta* strains, with the greatest variation observed for CBM (Fig. 4**B**). By percentage of all CAZymes identified, CH01 and CH02 are enriched for AA (16%, 16%), GH (48%, 50%), and GT (18%, 18%) compared to other strains, but feature the smallest proportion of CBM for all *Coniochaeta* strains, by approximately 2-fold. PR01 follows the trends of the *Coniochaeta* strains, but its proportions of CBM (8%) and GH (55%) are even more extreme than those of CH01 and CH02, with CBM proportions of 9% for both, and GH proportions of 48% and 50% in CH01 and CH02 respectively.

The distribution of CAZymes based on putative substrate was also considered. CAZyme classes were assigned to activity against lignin, cellulose, hemicellulose, or pectin using the class assignments specified in Table 1 (Fig. 4**C**). The general distributions are similar between all *Coniochaeta* strains, with 11 – 15% of CAZymes acting in lignin degradation, 8 – 10% for cellulose, 13 – 15% for hemicellulose, and 4 – 6% for pectin. Compared to all *Coniochaeta* strains, PR01 has a similar proportion of CAZy motifs active against lignin (12%), but slightly higher proportions of those active against cellulose (12%), hemicellulose (16%), and pectin (7%), resulting in a similar distribution but a larger overall proportion of the CAZy motifs dedicated to these four substrates.

Fungal proteomes, particularly those of pathogenic or saprophytic fungi, include rich secretomes to facilitate exodigestion (Lowe and Howlett, 2012). To predict how many CAZymes are secreted in CH01, CH02, and PR01, peptide signal sequences were analyzed using SignalP. Of the identified CAZyme genes, 193 (45%) are predicted to be secreted in CH01, 183 (43%) in CH02, and 179 (37%) in PR01. Most of these secreted CAZymes were detected as expressed in transcriptomic data for CH01 and PR01 (94% and 95%, respectively). Comparison of the CAZy motif distributions for all CAZymes identified with distributions for those that are expressed, or both expressed and secreted revealed that general trends are preserved between the distributions of all CAZymes and those that were expressed, but the distribution of the expressed and secreted CAZymes diverges from this pattern (Fig. 4**D**). These findings were confirmed using chi-squared analyses, according to which there is no significant difference in CAZyme distributions between 'identified' and 'expressed' sets (p-value > 0.95), but the difference between 'identified' and 'expressed and secreted' distributions is highly significant (p-value < 0.00001) for both CH01 and PR01. The main source of variation appears to be the relatively small proportion of secreted GTs; while 38 – 55% of the identified AA, CBM, CE, and GH CAZymes, and a striking 75–88% of PL CAZymes, are predicted to be secreted, fewer than 8% of GT CAZymes contained signal sequences for secretion. Precise counts for the discussed distributions of CAZymes and CAZy motifs are provided in Supplementary Tables 3–6.

In hopes of identifying specific environmental adaptions of strain CH01 to its hydrocarbon-rich environment, differences in CAZyme class abundances between both *C. hoffmannii* strains were investigated. The *C. hoffmannii* strains have nearly identical distributions (Fig. 4**A**), and all but 15 classes feature the same number of predicted proteins. These differing classes were individually investigated by pairing orthologs in CH01 and CH02 using BLAST and analyzing coding sequences for unmatched proteins to determine if they are unique to one strain or the other. From this process, a total of 15 CAZymes were identified as unique to either CH01 or CH02, as described in Table 3. Functional predictions were made based on functions of top BLAST and PSI-BLAST hits. Based on the strain-specific proteins identified, we predicted that CH01 should have stronger ligninase, beta-glucosidase, pectinase, xylanase, and feruloyl esterase activities than CH02, but CH02 should demonstrate greater amylase activity than CH01.

3.5. Codon Usage Bias and GC Content Characterization

A broad range of codon preferences and GC biases can be observed across fungal lineages (Wilken et al., 2020), and skews in GC content and codon usage have been shown to modulate gene expression at multiple levels (Zhou et al., 2016). GC content and preferred codons were identified for CH01, CH02, and PR01 genomes using the EMBOSS CUSP and CAI tools and CodonW. Results were then compared with transcriptomic data to determine how biases in codon usage and GC content may affect patterns of gene expression.

All three strains have strong GC biases, with coding sequence GC contents of 60.5% for CH01, 60.4% for CH02, and 59.0% for PR03. These coding sequence GC contents are close to those of *Aspergillus nidulans* (53.0%) and *Neurospora crassa* (56.3%), but markedly different from those of *Candida albicans* (36.9%), *Saccharomyces cerevisiae* (39.8%), *Schizosaccharomyces pombe* (39.8%), and *Kluyveromyces lactis* (40.1%) (Rice et al., 2000). This distinction between high and low GC content mirrors the evolutionary lineages of these model species, with low-GC members of the order *Saccharomycetales* (*C. albicans, K. lactis, S. cerevisiae)* and subphylum *Taphrinomycotina* (*S. pombe*) clustering separately from the high-GC members of the clade *leotiomyceta* (*A. nidulans, C. hoffmannii, N. crassa, P. richardsiae*). Analysis of position-specific GC content revealed that the wobble position is particularly polarized for all nine strains. CH01, CH02, and PR01 have wobble GC contents (GC3) at least 10% higher than their overall GC contents, with GC3 values of 75.6%, 75.2%, and 71.9% respectively (Fig. 5**A**).

To investigate whether average GC bias varies with expression level, GC content of the top 10% of genes with highest expression was analyzed in the strains with expression data (CH01 and PR01). When only highly expressed coding sequences were considered, statistically significant changes in the overall and position specific GC contents of CH01 and PR01 were observed (Fig. 5**B**). In CH01, the increases in overall GC and GC3, and the decreases in GC1 and GC2 were all found to be significant (with $p < 0.01$). Interestingly, GC1, GC2, and overall GC contents decreased significantly ($p < 0.01$) in PR01, but no significant

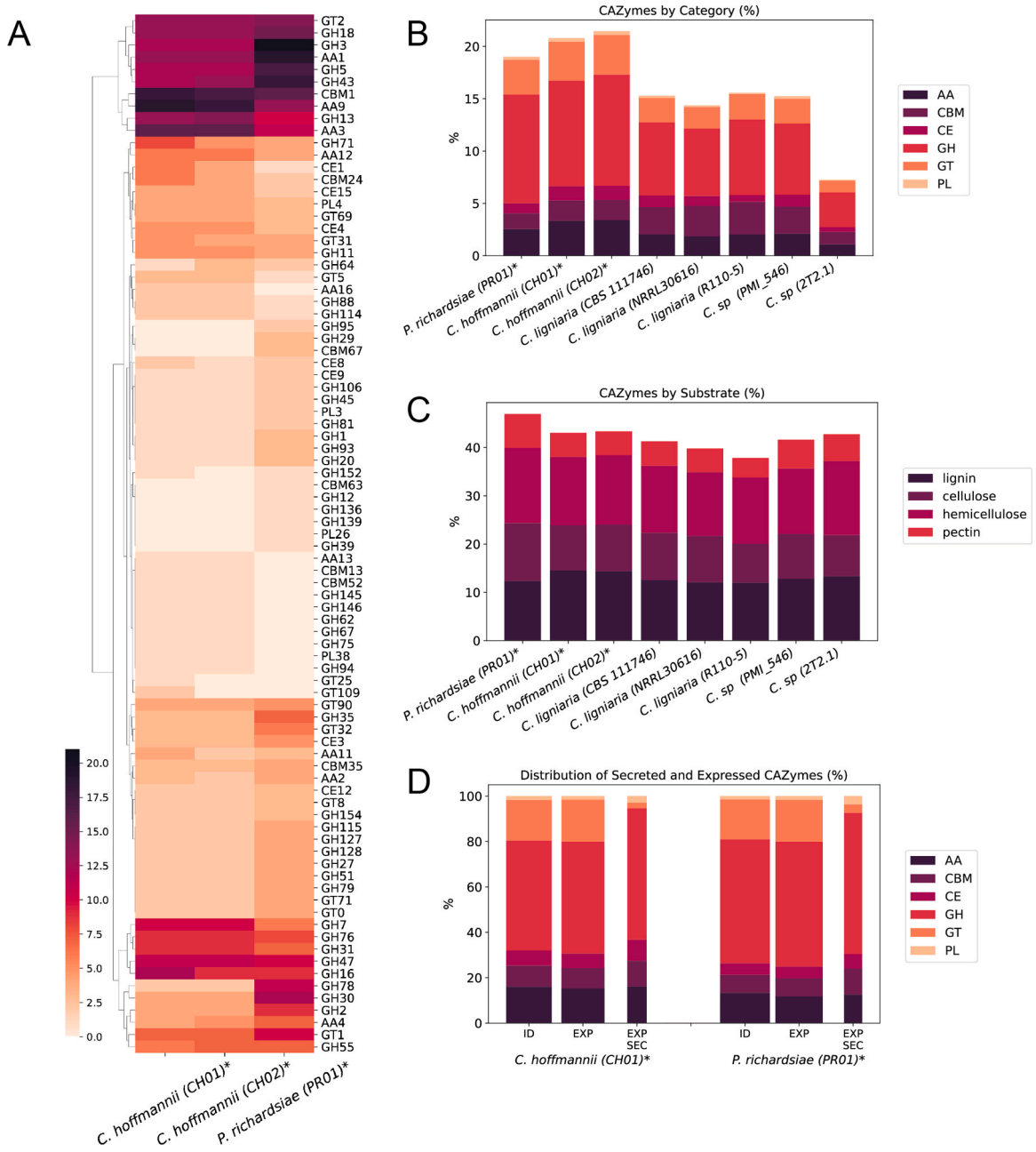

Fig. 4. *C. hoffmannii* and *P. richardsiae* CAZyme distributions show limited divergence from those of related species. (A) Class distributions of CAZy motifs in CH01, CH02, and PR01, with classes hierarchically clustered. Classes in which all three strains had identical counts are not shown here, but included in Supplementary Figure 1. (B, C) Distributions of CAZymes in CH01, CH02, PR01, and five other *Coniochaeta* strains based on category (B) and putative substrates (C). Values for (B) and (C) are presented as percentages of the total number of CAZy motifs identified in each respective strain. (D) Distribution of CAZy motifs in CH01 and PR01 by category for all motifs identified (Id), those that are expressed (Exp), and those that are both expressed and secreted (Exp Sec). Values in (D) are presented as percentages of the total number of motifs that were identified, expressed, or expressed and secreted for each strain as indicated, with column widths proportional to the number of motifs in each category. The CAZy categories are abbreviated auxiliary activities (AA), carbohydrate binding motifs (CBM), carbohydrate esterases (CE), glycoside hydrolases (GH), glycosyl transferases (GT), and polysaccharide lyases (PL).

change was noted for GC3. These results suggest that expression level corresponds more closely with GC3 content than with GC content in CH01. Indeed, expression levels have stronger correlations to GC3 content than to GC content for both strains based on Pearson's correlation coefficients (Fig. 5**C**). Although these relationships do not appear linear and are too weak for GC composition at any position to serve as an indicator of expression level, they confirm the relationship between expression and GC3 content is stronger than that with GC content, and reveal stronger correlations in CH01 than in PR01.

It is unsurprising that the values for GC3 content are more polarized than overall GC content across all strains analyzed, as the wobble effect confers additional flexibility for the nucleotide that occupies this third position. The elevated GC3 contents suggest this flexibility facilitates the high GC bias observed in CH01, CH02, and PR01 via preferential use of codons ending with G or C nucleotides. To investigate this possibility, codon usage was analyzed in coding sequences across all three strains and other model fungi. As with GC content, patterns of codon usage in CH01, CH02, and PR01 closely follow those of *A. nidulans* and *N. crassa,* but stand in sharp contrast to those of *C. albicans, S. cerevisiae*, *S. pombe*, and *K. lactis*. Unsupervised clustering of species based on codon usage

Table 3
Predicted CAZymes identified as unique to CH01 or CH02.

Gene ID:	Unique to Genome:	Class:	Expressed:	Secreted:	Top BLAST hit description:	PSI-BLAST frequent descriptions after 3 iterations:
g10224.t1	CH01	CE1	Y	Y	feruloyl esterase B	xylanase
g1074.t1	CH01	CE1	Y	Y	alpha/beta hydrolase	PHB depolymerase, feruloyl esterase
g1367.t1	CH01	CE8	Y	Y	pectinesterase	pectinase
g1640.t1	CH01	GT25	Y	N	hypothetical protein	galactosyl transferase
g1647.t1	CH01	GH16	Y	Y	GH16 protein	beta-glucosidase
g2388.t1	CH01	GH43	Y	Y	GH43 protein	xylanase
g3571.t1	CH01	AA9/CBM1	Y	N	GH16 protein	beta-glucosidase
g8518.t1	CH01	AA11	N	N	hypothetical protein	protease
g8675.t1	CH01	GH71	N	Y	hypothetical protein	alpha-glucosidase
g8678.t1	CH01	AA2	Y	N	Heme peroxidase	ligninase
g9409.t1	CH01	GT31	Y	Y	hypothetical protein	galactosyl transferase
g4634.t1	CH01	GH16	Y	Y	concanavalin-like lectin/glucanase	xylanase
g2549.t1	CH02	AA4		N	Hypothetical protein, GE09DRAFT	ligninase
g2909.t1	CH02	GH43		Y	GH43 protein	xylanase
g5370.t1	CH02	GH13		N	alpha-amylase	alpha-glucosidase

recreated taxonomic lineages with only minor differences in the placement of *N. crassa* (Fig. 5**D**). Although overall trends are preserved between CH01, CH02, and PR01, the species have several distinctions. Unsurprisingly, CH01 and CH02 have stronger biases towards GC bases in the wobble position than does PR01. The largest differences in codon usage are observed between the codons TAC and TAA (Tyr), AAC and AAT (Asn), and CAC and CAT (His), with frequencies varying between CH01 and PR01 by 5.6%, 7.4%, and 5.8% respectively. In each case, CH01 demonstrates the stronger preference for C in the wobble position. Little intraspecies variation in codon usage is observed, with preferences of CH01 and CH02 differing by less than 1% for all but two codons. These exceptions are the STOP codons TAG and TGA, for which frequencies vary by 2.4%, with CH02 demonstrating a heightened preference for TGA.

Codon usage frequencies in highly expressed genes were used to identify preferred codons. Without expression data for CH02, strain-specific preferences could not be determined. However, based on the similarity between the GC compositions and codon usage frequencies of CH01 and CH02 and general intraspecies conservation of codon preferences, values obtained for CH01 are expected to well-represent CH02 (LaBella et al., 2019). Using the species-specific codon preference values, the codon adaptation index (CAI) was calculated for each gene. CAI is a codon bias metric that measures how well-adapted a sequence is, given a particular set of preferred codons. Coding sequences using preferred codons have high CAI values, while those with sub-optimal codon usage are marked by low CAI values. Additionally, the effective number of codons (Nc) was calculated using CodonW. Nc is another codon bias metric, which captures the deviation of a sequence's codon usage from a random distribution. As optimized sequences are enriched for preferred codons and farther from a random distribution, they effectively use fewer codons and thus have lower Nc values.

For all three strains, the distributions of CAI and Nc values for coding sequences are approximately normal, with slight skews to the right for CAIs and to the left for Nc corresponding to more-optimized coding sequences (Fig. 6**A**). Compared to CH01 and CH02, PR01 demonstrates more skew for both CAI and Nc, and thus more-optimized sequences gauged by both metrics. CAI and Nc are negatively correlated for both strains, with Pearson's correlation coefficients of − 0.89 for CH01 and − 0.94 for PR01. Both metrics weakly correlate with expression, as Pearson's correlation coefficients for expression versus CAI and Nc were respectively 0.20 and − 0.18 for CH01, and 0.12 and − 0.11 for PR01 (Fig. 6**C,** Supplementary Figures 2 and 3). Correlations between codon bias metrics for CH01 and PR01 considering either all genes or only expressed genes were calculated, revealing strong correlations between metrics, but no strong correlations between metrics and expression levels for CH01 or PR01 (Supplementary Figures 4 and 5). While this may indicate codon usage bias is a poor indicator of expression in the conditions and strains tested, this could also be explained by the stage of regulation at which codon usage bias affects expression. While work in *N. crassa* has implicated codon optimization in controlling transcript abundance (Zhou et al., 2016), codon optimization is generally hypothesized to act through regulation of translation, which would not be accounted for in our transcriptomic analyses.

3.6. Characterization of Enzymatic Activities

To characterize the enzymatic activities exerted by CH01, CH02, and PR01 and investigate differences predicted based on genetic analysis, enzyme assays for amylase, beta-glucosidase, cellulase, chitinase, esterase, feruloyl esterase, gelatinase, laccase, pectinase, tannase, urease, xylanase, and caseinase activity were conducted. All three strains performed similarly on most assays, with positive results for each in the amylase, beta-glucosidase, cellulase, esterase, pectinase, urease, xylanase, and caseinase assays (Fig. 7**A**). All three strains also demonstrated the ability to assimilate *n*-hexadecane and mineral oil (data not shown). Differences between strains were observed for chitinase, feruloyl esterase, gelatinase, laccase, and tannase activities (Fig. 7**B**). Solely strain CH01 lacks chitinase and gelatinase activity, while PR01 lacks laccase activity, and both CH01 and CH02 lack feruloyl esterase and tannase activities.

The enzymatic index (EI) was calculated for the quantitative clearance-based amylase, pectinase, cellulase, and caseinase assays, providing additional information beyond the simple classification as positive or negative (Fig. 7**D**). PR01 demonstrates significantly ($p < 0.05$) higher pectinase activity than CH01, and CH02 demonstrates greater cellulase activity than PR01. Based on *in silico* CAZyme analysis, CH01 was expected to outperform CH02 in the pectinase assay, and CH02 was expected to outperform CH01 in the amylase assay, but no statistically significant differences were detected between CH01 and CH02.

4. Discussion

After screening candidate strains from the Culture Collection Ex that were isolated in hydrocarbon contaminated environments, two fungal species which appeared to grow well on plastic fibers were identified as *Coniochaeta hoffmannii* and *Pleurostoma richardsiae*. These isolates were then characterized using experimental and bioinformatic approaches to assess activities against a variety of synthetic and naturally occurring compounds, including PP, and to compare their genomes with those of closely related species.

As revealed through light and SE microscopy, *C. hoffmannii* and *P. richardsiae* were able to wrap themselves around synthetic fibers and utilize pure PP as the sole carbon source (Figs. 1, 2). Excessive growth was observed for both *C. hoffmannii* and *P. richardsiae*, with distinct patterns of colonization. *C. hoffmannii* spread across almost the whole

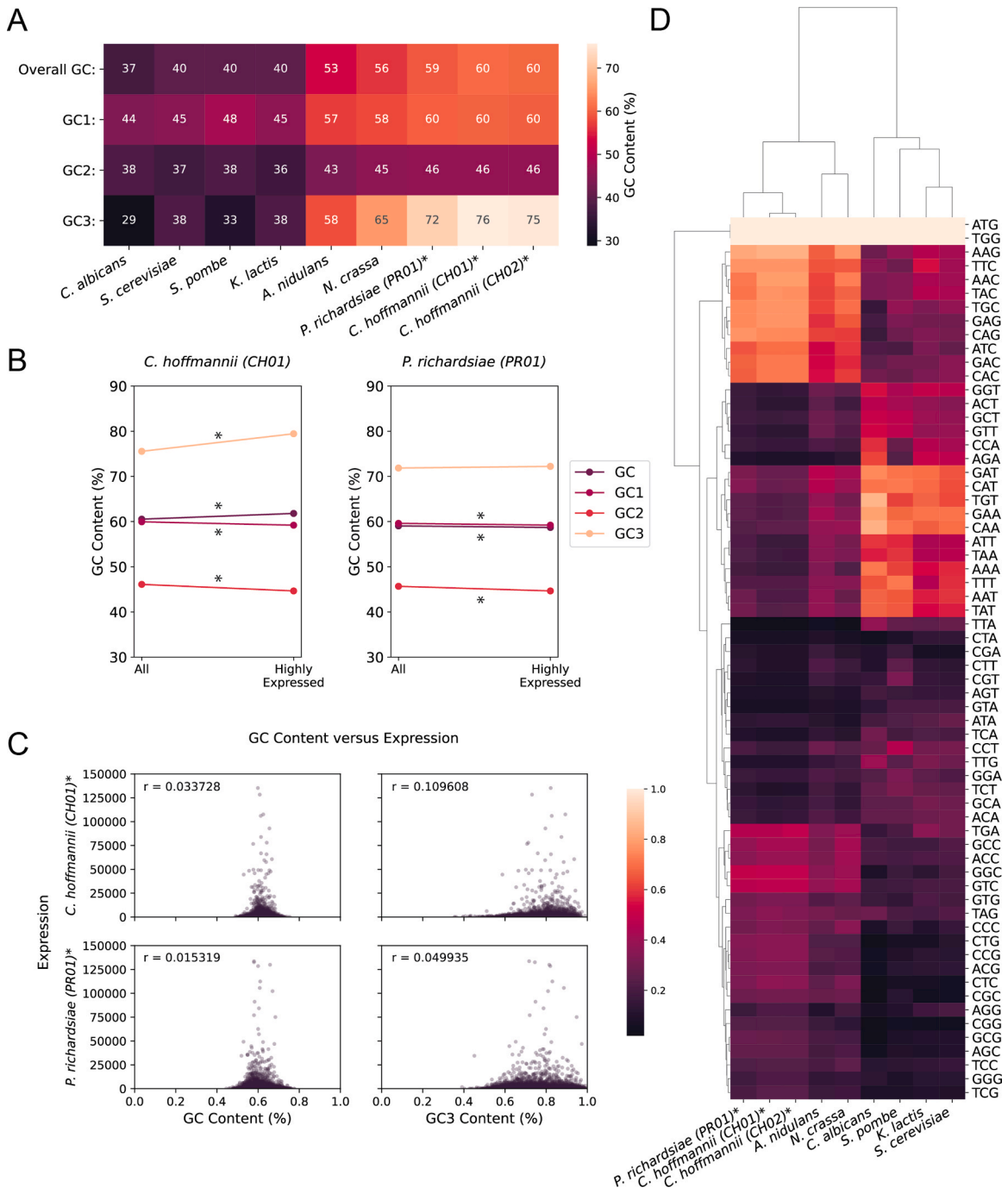

Fig. 5. GC and GC3 content varies across fungal lineages and expression levels. (A) Overall and position-specific GC content (by %) in CH01, CH02, PR01, and selected model fungi. (B) Overall and position specific GC content in CH01 and PR01 for all coding sequences versus highly expressed coding sequences. Significant differences as determined by bootstrap analysis are indicated (* = $p < 0.01$). (C) GC (left) and GC3 (right) content versus expression level for all expressed genes in CH01 (top) and PR01 (bottom) with Pearson's correlation coefficients shown. (D) Codon usage frequencies for all coding sequences in CH01, CH02, PR01, and selected model fungi. Both rows and columns are hierarchically clustered to discern overall patterns of usage between the strains.

portion of PP film, while the growth of *P. richardsiae* was more localized around the inoculation site but was still significant. As shown by SEM of PP films, only a few hyphae of *P. richardsiae* were observed beyond 0.5 mm from the edge of inoculation (marked by a green cross, Fig. 2). In contrast, *C. hoffmannii* spread very intensely, with hyphae noticeable over 2.0 mm away from the edge (marked with blue cross, Fig. 2). There are few SEM photos of fungi on plastic films in the literature (e.g., *Penicillium oxalicum*, and *Penicillium chrysogenum* on polyethylene films, *Aureobasidium pullulans* on polyvinyl chloride, and fungal biofilms on polyurethane (Barratt et al., 2003; Ojha et al., 2017; Webb et al., 2000)), but to our knowledge none on PP fibers or films.

PP is a non-hydrolysable polymer with a high hydrophobic character due to the presence of hydrocarbons and methyl groups on the side chain of polymer backbone (Jeon and Kim, 2016; Rana et al., 2022). Raman spectroscopy has been used previously to detect changes in polyethylene after incubation with various bacteria (Peixoto et al., 2017), but for PP it has been used mainly with a focus on abiotic degradation (Dong et al., 2020; Phan et al., 2022). The chemical changes of PP film during the colonization were analyzed using Raman spectroscopy, as shown in Fig. 2. Differences between spectra for colonized and uncolonized PP

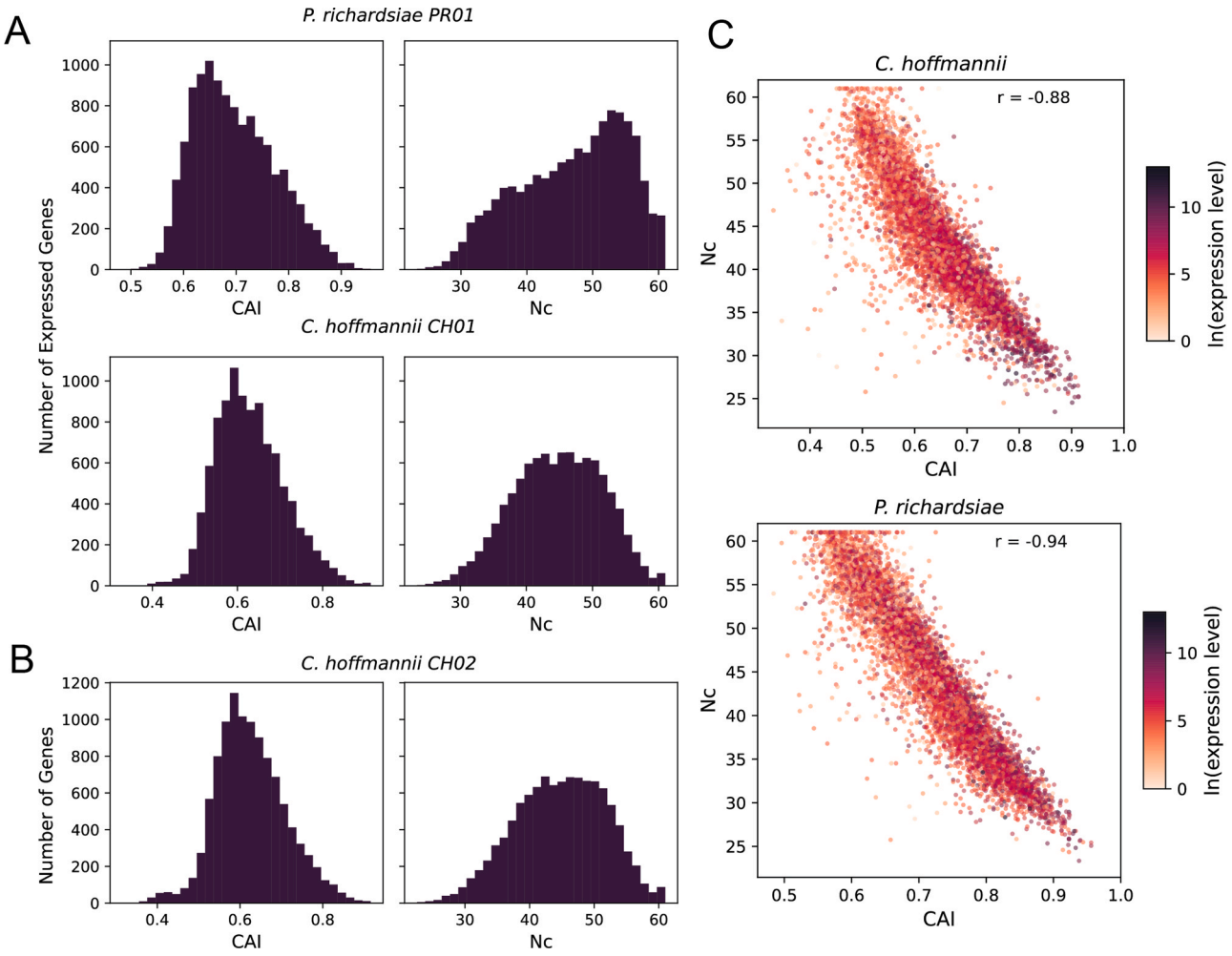

Fig. 6. Codon optimization varies with, but does not explain, transcript abundance in CH01 and PR01. (A, B) Distributions of codon adaptation index (CAI) and effective number of codons (Nc) values for expressed genes in CH01 and PR01 (A), and all genes in CH02 (B). (C) Scatter plots of CAI values versus Nc values for expressed genes in CH01 and PR01. Points are colored based on the natural log of the expression level, and Pearson's correlation coefficients for CAI and Nc are shown for each plot.

films are noticeable in the relative intensity of the peak at 2889 cm^{-1}, which corresponds to symmetric stretching of the -CH_3 group in PP polymer (Guo et al., 2019; Mei et al., 2022). Intensity of this particular band increased for PP colonized with *C. hoffmannii* and decreased for PP colonized with *P. richardsiae*, indicating a relative increase and decrease of -CH_3 groups, compared to the pure PP film. Additionally, for the *P. richardsiae*, a decrease in the intensity of the peaks at 401 and 812 cm^{-1} was observed, which is associated with CH bonds although not exclusively. For *C. hoffmannii* the spectrum shows an opposite trend, the absorption peaks increase. Considering that the observed changes are relative, the conclusion made from the analysis has to include the possibility that both exposed samples exhibit the decrease of also all the carbon-carbon bonds. This implies that in the sample treated by the *P. richardsiae* even more CH bonds would be depleted, whereas in the *C. hoffmannii* sample, some new CH groups would be formed. Our findings support this possibility as a new broad peak appearing at 1600 cm^{-1} (1655 and 1545 cm^{-1}) which can be associated with the C═C bond formation. This is consistent with formation of polyisoprene, which would have a double C═C bond (with the identical energy of vibration), at the expense of one -CH_2 group (Gomez et al., 2019). Similar to our findings, Yang et al. (Yang et al., 2021) identified C═C bond formation in PP biodegraded by gut microbes with a diverse microbiome, using FTIR spectroscopy. There is also a study that analyzed the degradation of PP by endophytic fungi (Sheik et al., 2015). However, in this study, the films of PP were irradiated with gamma rays before inoculation of the fungal strains, so it is difficult to compare the results. In other studies that investigated the degradation of plastics by fungi with FTIR, only polyethylene films were analyzed (Bonhomme et al., 2003; Ojha et al., 2017).

Based on Raman spectroscopy and FTIR-ATR, both fungi alter some characteristic bonds of PP. While *C. hoffmannii* treatment led to variations in -CH absorbance at different wavenumbers in Raman spectroscopy and FTIR-ATR *P. richardsiae* treatment demonstrated marked decreases in CH_3, C-C, and CH_2 absorbances, as suggested by FTIR-ATR, and leads to the formation of C═C bonds as suggested by Raman spectroscopy. The results also indicate that *C. hoffmannii* produced a more spatially homogeneous polypropylene degradation than that produced by *P. richardsiae*.

The primary mechanism for the biodegradation of high molecular weight polymer is the oxidation or hydrolysis by enzymes creating functional groups that improve its hydrophilicity (Rana et al., 2022). Apparently only *P. richardsiae* was able to decrease the intensity of CH_3C-C bond, probably by changing the polymer by β-oxidation of the chains of carbonyls and consequently, decreasing the intensity of the band at 898 cm^{-1}. But both fungi produced a clear increase in carbonyl absorbance (Fig. 3C and Table 2), suggesting significant oxidation. Presently, there are no other studies describing the capabilities of *C. hoffmannii* and *P. richardsiae* to degrade polypropylene. However,

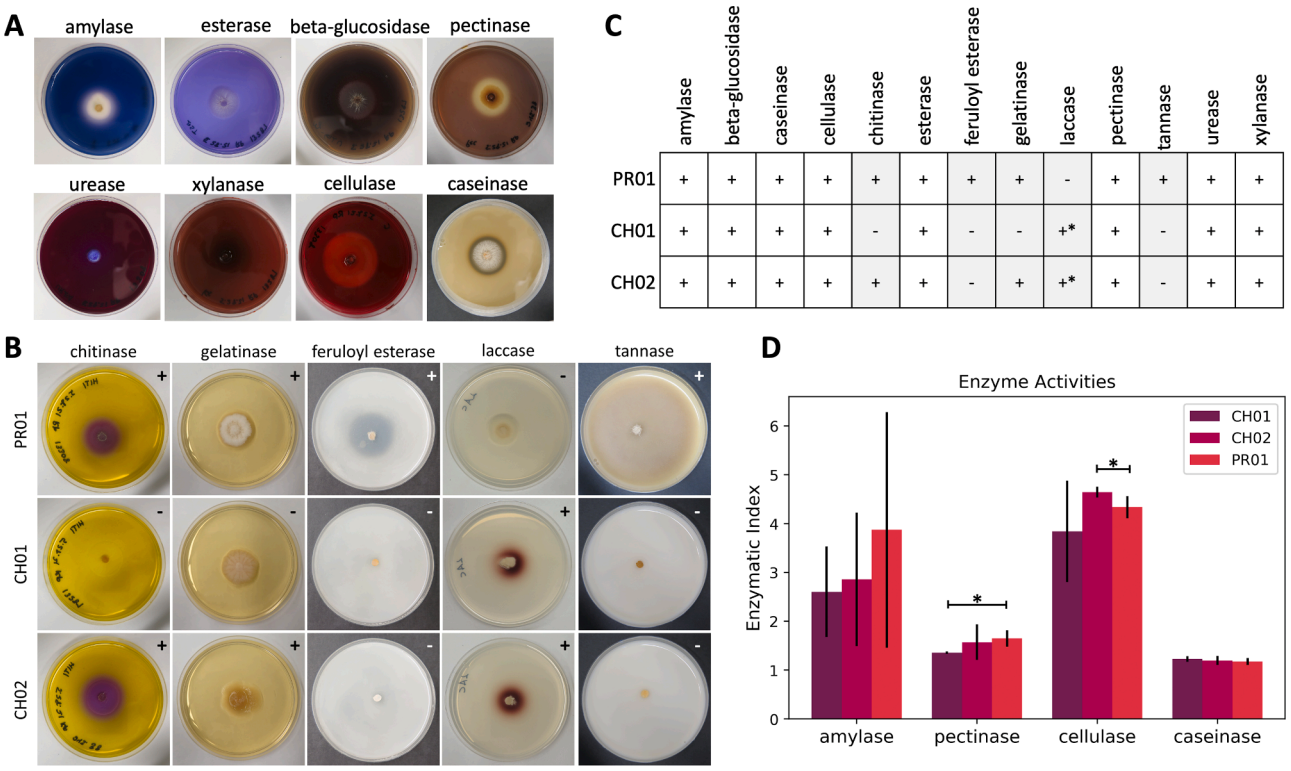

Fig. 7. Enzymatic activities of *C. hoffmannii and P. richardsiae*. (A) Representative media with positive results are shown for assays in which all three strains were positive, namely, the amylase, esterase, beta-glucosidase, pectinase, urease, xylanase, cellulase, and caseinase assays. (B) Results for assays in which strains differed, namely the chitinase, gelatinase, feruloyl esterase, laccase, and tannase assays. The upper right corner of each pane indicates whether the result was positive or negative. (C) Performance of all three strains in each enzyme activity assay. Grey shading indicates enzymatic activities that differed between strains. Assays were conducted with n = 3, except for pectinase (n = 2) and laccase (n = 9) assays. All replicates yielded the same results unless indicated by * . For the laccase assay, CH01 tested positive in 7 of 9 replicates and CH02 tested positive in 6 of 9 replicates. (D) Mean enzymatic indices of the assays for which EI could be quantified according to Eq. 1 in Methods. Error bars indicate 95% confidence intervals for three replicates for amylase, cellulase, and caseinase, and two replicates for pectinase. Significant differences ($p < 0.05$) are indicated by * .

some fungal strains such as *Aspergillus fumigatus*, have been shown to degrade impure PP polymers (Oliya et al., 2020), resulting in increased C-H vibration together with formation of C═O, the aldehyde group, after 4 months of treatment, and increased stretching of CH_3 group at 1450.52 cm^{-1} after 6 months of fungal incubation.

After observing the activities of each strain against pure PP, whole genome and transcriptome sequencing were conducted. The genomes of both *Coniochaeta hoffmannii* EXF-13287 and *Pleurostoma richardsiae* EXF-13308 were of expected size compared to genomes of their close relatives. Both genomes were relatively compact, with little repetitive DNA. The number of predicted genes met expectations, and the genome sequences and annotations for both were close to complete. While other strains of *C. hoffmannii* have been sequenced previously (Leonhardt et al., 2018), to the best of our knowledge, this is the first whole-genome sequencing of *P. richardsiae*.

Altogether, the CAZyme classification data for *Coniochaeta hoffmannii* and *Pleurostoma richardsiae* describe typical proteomes for wood rot fungi. When compared to related *Coniochaeta* strains, both analyzed *C. hoffmannii* strains had relatively low numbers of CAZy motifs, with totals of 481 and 466 compared to values of 642, 654, 656, 696, and 1378 for *Coniochaeta* sp. and *Coniochaeta ligniaria* strains (Grigoriev et al., 2012; Jimenez et al., 2017; Mondo et al., 2019; Nelson et al., 2022; Nordberg et al., 2014). This variation can likely be ascribed to discrepancies in the sensitivity and stringency of genome annotation and CAZyme identification. In our analysis, only CAZymes identified by at least two of the three prediction programs in dbCAN2 were considered significant and investigated further in order to strengthen our confidence in functional predictions. When all CAZy motifs identified using dbCAN2 are considered significant rather than only those identified by at least two programs, the counts for CH01 and CH02 increase to 652 and 630, in line with the values for related *Coniochaeta* strains (with the exception of *Coniochaeta* sp. 2T2.1, which has 1378 reported CAZy motifs and seems to have undergone a recent duplication event) (Mondo et al., 2019).

The distributions of CAZy motifs based on classification were also compared between *Coniochaeta* species. Both *C. hoffmannii* strains have relatively high proportions of auxiliary activities (AA), glycoside hydrolase (GH), and glycosyl transferase (GT) motifs, balanced by low proportions of carbohydrate binding motifs (CBM). This result could be explained by heterogeneity in CBMs resulting from environment-specific adaptations. Recycling of CBMs to recognize new substrates or loss of selective pressure to recognize carbohydrates could occur in hydrocarbon-rich environments, potentially facilitating degradation of synthetic polymers including polypropylene. The resulting divergent or degenerate sequences may then be missed by CBM recognition, resulting in their exclusion from our CAZyme datasets. Limited data on other *Pleurostoma* species and strains precluded detailed comparisons of *P. richardsiae* with close relatives, but CAZyme abundance and distributions in the strain generally followed patterns of *Coniochaeta* species. Future sequencing and characterization of related *Pleurostoma* species will hopefully provide a wider context for the genus and potentially reveal specific adaptations of *P. richardsiae*.

Wood-rot fungi are rich in enzymes for degradation of lignin, cellulose, hemicellulose, and pectin. While white-rot fungi tend to specialize in lignin degradation, soft-rot fungi are enriched for cellulolytic, hemicellulolytic, and pectinolytic enzymes (Sista Kameshwar and Qin, 2018). Analysis of CAZyme distributions based on putative substrate revealed over 40% of the CAZymes in *C. hoffmannii* and *P. richardsiae*

likely target one of these four substrates, with the largest proportions targeting hemi-cellulose, then lignin. This is consistent with described roles of *Coniochaeta* species and *P. richardsiae* as wood-rot fungi, but suggests an intermediate behavior between soft-rot and white-rot (Lawrence et al., 2021; Leonhardt et al., 2018).

Comparison of expressed and secreted CAZyme distributions in CH01 and PR01 revealed that CAZyme composition of the secretomes differs substantially from overall CAZyme distributions. While the profiles of expressed CAZymes closely followed those for all identified CAZymes, the distributions of CAZymes that were both expressed and secreted were significantly depleted of GT motifs for both strains. This finding suggests that GTs are underrepresented in the secretomes, and glycosyl transferase activity may play a larger role in intracellular processes than in exodigestion. However, the similarity between identified and expressed CAZyme distributions confirms that CAZyme prediction alone can accurately depict enzymatic profiles.

While plastic degradation activity has been attributed to a diverse range of microorganisms, there are relatively few studies linking these broad activities to specific enzymes (Kaushal et al., 2021). Most known plastic-degrading enzymes are classified as esterases, cutinases, or lipases, all of which fall under the enzyme class of hydrolases (Danso et al., 2018; Gaytan et al., 2019; Kang et al., 2011; Mayumi et al., 2008; Muller et al., 2017; Pinnell and Turner, 2019; Popovic et al., 2017; Sulaiman et al., 2012; Tchigvintsev et al., 2015). Hydrolases cleave large compounds into smaller pieces by cleaving chemical bonds, consuming water molecules in the process. Most of the enzymes known to degrade plastics are active against polymers that include carbonyl groups, such as polyethylene terephthalate, polylactic acid, polybutylene succinate, polyhydroxy butyrate, and polycaprolactone. Notably fewer enzymes have been found to degrade the highly hydrophobic polymers of polyethylene, and none have been found to degrade PP (Kaushal et al., 2021).

Several bioinformatic tools have been developed to identify putative plastic-degrading enzymes based on homology to the few that have been characterized (Danso et al., 2018; Sankara Subramanian et al., 2020). While this approach is useful for identifying candidate genes from sequences such as metagenomic datasets (Danso et al., 2018; Gaytan et al., 2019; Pinnell and Turner, 2019), it fails to identify novel enzymes. Without existing characterization of PP-degrading enzymes, these predictive programs are not expected to aid our search for the enzymes responsible for biodegradation by *C. hoffmannii* and *P. richardsiae*. To identify enzymes that contribute to PP degradation activity, proteomic and biochemical approaches will be needed.

Rather than combing the genomes for sequences homologous to known plastic degrading enzymes, we analyzed the predicted proteomes and enzymatic activities of these two strains to broadly compare their behaviors to related strains and species. Although both *C. hoffmannii* strain CH01 and *P. richardsiae* were isolated from hydrocarbon-rich environments and demonstrated the ability to degrade polypropylene, their predicted proteomes show limited divergence from related species. However, it is entirely possible other isolates of these species are also capable of degrading hydrocarbons. As the holotype of *C. hoffmannii* was isolated from butter (Weber, 2002) and *P. richardsiae* frequently infects olive trees (Canale et al., 2019; Lawrence et al., 2021), it is possible these species are already well adapted to hydrocarbon-rich environments, and relatively little adaptation would be required to grow on or utilize synthetic polymers. While many studies have investigated fungi isolated in hydrocarbon contaminated environments (Hassan Sel et al., 2014; Jones et al., 1970; Leahy and Colwell, 1990), specific characterization of genomic and proteomic adaptation is lacking. Interestingly, entomopathogenic fungi that assimilate hydrocarbons from the outer layer of insect cuticles appear to have increased P450 monooxygenases and acyl-CoA enzymes, as well as increased superoxide-dismutase and catalase activity, allowing them to metabolize hydrocarbons and handle the oxidative stress stemming from beta-oxidation (Huarte-Bonnet et al., 2015). Further work is needed to determine if these strategies are specific to insect-derived hydrocarbons or general, and can be leveraged against synthetic hydrocarbons.

The possibility that these species are primed to utilize hydrocarbons is supported by the growth of CH01, CH02, and PR01 in mineral oil and *n*-hexadecane assimilation assays. Thorough assessment of polymer degrading activities in related strains and species is needed to tell if these abilities are widely observed in related fungi, general to the species, or unique to strains CH01 and PR01. Strain specific degradation is not inconsistent with the highly similar CAZyme profiles and general conservation across strains, as even slight changes in coding sequences could modulate protein activity without disrupting bioinformatic identification of a protein or CAZy motif. Many CAZymes are inherently promiscuous, so even small mutations could be sufficient for adaptation to new substrates (Pallister et al., 2020). Additionally, changes in expression level could drive adaptation. While mutations in regulatory regions could account for altered expression levels, changes in GC content and codon usage may also contribute to modulated patterns of expression.

The coding sequences of *P. Richardsiae* and both *C. hoffmannii* strains demonstrated acute GC preferences and codon usage biases. The preferences observed were similar to, but generally more extreme, than those of *Aspergillus nidulans* and *Neurospora crassa*, and distinct from preferences observed in *Candida albicans, Saccharomyces cerevisiae, Schizosaccharomyces pombe*, and *Kluyneromyces lactis* (Edelmann and Staben, 1994; Ene et al., 2019; Lloyd and Sharp, 1991; Rice et al., 2000; Wood et al., 2002). These relationships between GC and codon biases closely follow the evolutionary history of these species, and hierarchical clustering of these strains based on codon preferences largely reflects their phylogenetic history (Naranjo-Ortiz and Gabaldon, 2019). Of all species analyzed, *C. hoffmannii* had the highest GC content overall (GC) and wobble position GC content (GC3). Weak correlations between both GC and GC3 contents with expression level were noted in *C. hoffmannii*, and to a lesser extent in *P. richardsiae*. Together, the marked GC preference and slightly stronger correlation with expression in *C. hoffmannii* suggest modulation of GC composition may play a larger role in regulation of *C. hoffmannii* than that of *P. richardsiae*. Expression data for *C. hoffmannii* strain CH02 is needed to determine whether the observed relationship between GC content and expression is strain specific or general to the species. Codon usage bias, assessed with two different metrics, is also loosely correlated with expression, but the correlation coefficients were notably lower than published values for *N. crassa* (Zhou et al., 2016). Differences in the stage of regulation could account for this discrepancy. Codon usage bias was initially hypothesized to affect expression translationally, in accordance with tRNA abundances. However, work in *N. crassa* surprisingly revealed that codon usage modulates protein abundances largely by altering levels of transcription (Zhou et al., 2016). Simultaneous analysis of transcript and protein abundances is needed to determine if and when codon usage bias modulates gene expression in *C. hoffmannii* and *P. richardsiae*.

Enzymatic assays were used to characterize activities of each strain and test functional predictions based on bioinformatic analyses. The positive results for all three strains on assays for amylase, beta-glucosidase, cellulase, pectinase, and xylanase activities are unsurprising, given the role of these species as wood rot fungi and plant pathogens (Lawrence et al., 2021; Leonhardt et al., 2018). *P. richardsiae* uniquely demonstrated tannase and feruloyl esterase activities, suggesting it is capable of metabolizing tannins and cleaving ester linkages between the phenolic compound ferulic acid and carbohydrates in plant cell walls (Underlin et al., 2020). While both *C. hoffmannii* strains lacked feruloyl esterase and tannase activities, each possessed laccase activity, which was absent in *P. richardsiae*. Like feruloyl esterases, laccases contribute to mineralization of lignin and other plant cell wall components, so these findings suggest *C. hoffmannii* and *P. richardsiae* may leverage different strategies for invading plant tissues (Bourbonnais and Paice, 1990).

C. hoffmannii and *P. richardsiae* demonstrated degradation of the animal products urea, casein, and gelatin and the ability to grow at 37 °C

(Supplementary Figure 6), suggesting pathogenic potential (although CH01 lacks gelatinase activity). Indeed, both species have been identified as culprits in human infection in rare cases (Levenstadt et al., 2012; Marriott et al., 1997).

Both *C. hoffmannii* strains behaved similarly in enzymatic assays, and only chitinase and gelatinase activities differed between them. CH01′s inability to degrade chitin was surprising given the positive results of CH02 and PR01, but this potentially suggests CH01 lost chitinase function as the strain adapted to a hydrocarbon-rich environment. The negative result for gelatinase activity in CH01 was also intriguing given its positive result for the caseinase activity. Variations in the amino acid composition, size, and structures of casein and gelatin may underly this difference, but more information regarding the precise mechanism of degradation of each is needed (Eastoe, 1955, 1957; Lauer and Baker, 1977).

The functional predictions for CH01 and CH02 based on CAZyme abundance were not confirmed by enzymes assays. Based on analysis of unique CAZymes, CH01 was expected to outperform CH02 in ligninase, beta-glucosidase, xylanase, feruloyl esterase, and pectinase activities, and CH02 was expected to outperform CH01 in the amylase assay. Of these, only the pectinase and amylase assays yielded graded responses, and neither difference between CH01 and CH02 was statistically significant. Functional predictions could be further tested by increasing the statistical power of assays and using quantitative ligninase, beta-glucosidase, xylanase, and feruloyl esterase assays. However, as these predictions were based sheerly on gene number, they neglected possible differences in transcriptional and post-transcriptional regulations as well as the performance of individual enzymes and are thus highly oversimplified.

Based on these enzyme assays, all three strains demonstrated esterase activity. Most plastic-degrading enzymes, including lipases and cutinases, are classified as esterases (Kaushal et al., 2021), which was reflected, in part, in the positive results for esterase activity. However, PP chains do not include ester groups, and it is unknown whether esters are introduced into the chains throughout the process of biodegradation. In order to connect the broad enzymatic activities of these fungi to their PP-degrading activities, more knowledge of the mechanisms of PP degradation is needed. Sequencing and characterization of *Coniochaeta hoffmannii* and *Pleurostoma richardsiae* isolates from hydrocarbon-contaminated environments revealed limited divergence from related strains and species. The overall similarity of CAZyme profiles between *Coniochaeta* and *P. richardsiae* strains, coupled with their similar enzymatic activities and utilization of mineral oil and *n*-hexadecane hints that adaptation to hydrocarbon usage may be general to these species, rather than strain specific. As *C. hoffmannii* and *P. richardsiae* have been isolated in butter and olive trees respectively, it is conceivable that these strains are generally well adapted to hydrophobic environments and possess enzymes for hydrocarbon utilization which confer activity against PP across the species. It is also possible that this environmental adaptation did not lead to PP degradation, but rather poised the species to evolve this activity with relative ease, perhaps through slight modification of a promiscuous enzyme. In this case, we would expect PP degrading activity to be unique to the isolates CH01 and PR01. Further work characterizing related *Coniochaeta* and *Pleurostoma* species and strains is needed to differentiate between these possibilities, but in each case, it appears that species native to hydrocarbon-rich environments are predisposed for adaptation to plastic polymer usage and can serve as excellent candidates for future screens. Indeed, many enzymes capable of degrading synthetic polymers were initially identified in environments enriched in naturally occurring or synthetic polymeric substances, including compost, marine plastic samples, and landfills (Gaytan et al., 2019; Kang et al., 2011; Mayumi et al., 2008; Pinnell and Turner, 2019; Sulaiman et al., 2012; Zhu et al., 2022). Further sampling across diverse environments, particularly those rich in hydrocarbons, may uncover novel mechanisms for biodegradation and expand our limited set of plastic depolymerizing motifs. The *C. hoffmannii* and *P. richardsiae* isolates described here are extraordinarily promising for PP degradation, as the first reported fungi to demonstrate growth on additive-free, un-treated PP. Further work is needed to precisely quantify the PP-degrading activity of these strains and uncover the enzymes involved for potential applications in PP waste management, whether for biodegradation of environmental pollution or circularization of the PP economy.

CRediT authorship contribution statement

Rachel Porter: Software, Investigation, Formal analysis, Writing – original draft, Writing – review & editing, Visualization, Funding acquisition. **Anja Černoša**: Conceptualization, Methodology, Formal analysis, Investigation, Writing – original draft, Writing – review & editing, Visualization, Funding acquisition. **Paola Fernández-Sanmartín:** Investigation, Validation, Writing – review & editing. **Antonio Martínez Cortizas:** Formal analysis, Resources, Writing – review & editing, Funding acquisition. **Elisabet Aranda:** Formal analysis, Resources, Writing – review & editing. **Yonglun Luo:** Resources, Writing – review & editing, Funding acquisition. **Polona Zalar**: Investigation, Resources, Writing – review & editing, Funding acquisition. **Matejka Podlogar:** Investigation, Visualization, Writing – review & editing, Funding acquisition. **Nina Gunde-Cimerman**: Conceptualization, Resources, Writing - review & editing, Funding acquisition. **Cene Gostinčar:** Conceptualization, Methodology, Software, Formal analysis, Writing - review & editing, Supervision, Project administration, Funding acquisition.

Data Availability

All genomes and raw sequences are deposited to public database and accession number is mentioned in the manuscript.

Acknowledgements

This study was supported by funding from the Slovenian Research Agency to Infrastructural Centre Mycosmo (MRIC UL, I0-0022), programmes P2–0084, P4–0432, and P1–0198, project J4–2549 and L2–1830, the Young Researcher Grant to A. Černoša, the National Science Foundation Graduate Research Fellowship to R. Porter (DGE-1656518), and the Fulbright U.S. Student Program, sponsored by the U. S. Department of State. Contents are solely the responsibility of the author and do not necessarily represent official views of the Fulbright Program or US government. FTIR-ATR analyses were supported by funding by Xunta de Galicia (Grupos de Referencia Competitiva ED431C 2021/32). We acknowledge the CENN Nanocenter for the use of the Confocal Raman spectrometer. EA acknowledges Spanish Ministry of Science and Innovation MCIN/AEI/PID2021–123164OB-I00/FEDER Una Manera de hacer Europa).

Appendix A. Supporting information

Supplementary data associated with this article can be found in the online version at doi:10.1016/j.micres.2023.127507.

References

Ali, M.I., Ahmed, S., Robson, G., Javed, I., Ali, N., Atiq, N., Hameed, A., 2014. Isolation and molecular characterization of polyvinyl chloride (PVC) plastic degrading fungal isolates. J. Basic Microbiol. 54, 18–27.

Almagro Armenteros, J.J., Tsirigos, K.D., Sonderby, C.K., Petersen, T.N., Winther, O., Brunak, S., von Heijne, G., Nielsen, H., 2019. SignalP 5.0 improves signal peptide predictions using deep neural networks. Nat. Biotechnol. 37, 420–423.

Altschul, S.F., Gish, W., Miller, W., Myers, E.W., Lipman, D.J., 1990. Basic local alignment search tool. J. Mol. Biol. 215, 403–410.

Altschul, S.F., Madden, T.L., Schaffer, A.A., Zhang, J., Zhang, Z., Miller, W., Lipman, D.J., 1997. Gapped BLAST and PSI-BLAST: a new generation of protein database search programs. Nucleic Acids Res. 25, 3389–3402.

Alvarez Fernandez, N., and Matrinez Cortizas, A. (2022). 'andurinha': Make Spectroscopic Data Processing Easier (Comprehensive R Archive Network).
Asemoloye, M.D., Marchisio, M.A., Gupta, V.K., Pecoraro, L., 2021. Genome-based engineering of ligninolytic enzymes in fungi. Microb. Cell. Fact. 20, 20.
Auta, H.S., Emenike, C.U., Jayanthi, B., Fauziah, S.H., 2018. Growth kinetics and biodeterioration of polypropylene microplastics by Bacillus sp. and Rhodococcus sp. isolated from mangrove sediment. Mar. Pollut. Bull. 127, 15–21.
Barnes, D.K., Galgani, F., Thompson, R.C., Barlaz, M., 2009. Accumulation and fragmentation of plastic debris in global environments. Philos. Trans. R. Soc. Lond. B Biol. Sci. 364, 1985–1998.
Barratt, S.R., Ennos, A.R., Greenhalgh, M., Robson, G.D., Handley, P.S., 2003. Fungi are the predominant micro-organisms responsible for degradation of soil-buried polyester polyurethane over a range of soil water holding capacities. J. Appl. Microbiol 95, 78–85.
Bezalel, L., Hadar, Y., Cerniglia, C.E., 1997. Enzymatic mechanisms involved in phenanthrene degradation by the white rot fungus pleurotus ostreatus. Appl. Environ. Microbiol. 63, 2495–2501.
Bonhomme, S., Cuer, A., Delort, A.M., Lemaire, J., Sancelme, M., Scott, G., 2003. Environmental biodegradation of polyethylene. Polym. Degrad. Stab. 81, 441–452.
Bourbonnais, R., Paice, M.G., 1990. Oxidation of non-phenolic substrates. An expanded role for laccase in lignin biodegradation. FEBS Lett. 267, 99–102.
Brizzio, S., Turchetti, B., de Garcia, V., Libkind, D., Buzzini, P., van Broock, M., 2007. Extracellular enzymatic activities of basidiomycetous yeasts isolated from glacial and subglacial waters of northwest Patagonia (Argentina). Can. J. Microbiol 53, 519–525.
Buchfink, B., Reuter, K., Drost, H.G., 2021. Sensitive protein alignments at tree-of-life scale using DIAMOND. Nat. Methods 18, 366–368.
Busk, P.K., Pilgaard, B., Lezyk, M.J., Meyer, A.S., Lange, L., 2017. Homology to peptide pattern for annotation of carbohydrate-active enzymes and prediction of function. BMC Bioinform. 18, 214.
Cacciari, I., Quatrini, P., Zirletta, G., Mincione, E., Vinciguerra, V., Lupattelli, P., Giovannozzi Sermanni, G., 1993. Isotactic polypropylene biodegradation by a microbial community: physicochemical characterization of metabolites produced. Appl. Environ. Microbiol 59, 3695–3700.
Canale, M.C., Nunes Nesi, C., Falkenbach, B.R., Hunhoff da Silva, C.A., Brugnara, E.C., 2019. Pleurostomophora richardsiae associated with olive tree and grapevine decline in Southern Brazi. Phytophathol. Mediterr. 58, 201–206.
Cavalcanti, R.M.F., Ornela, P.H.O., Jorge, J.A., Guimarães, L.H.S., 2017. Screening, selection and optimization of the culture conditions for tannase production by endophytic fungi isolated from caatinga. J. Appl. Biol. Biotechnol. 5, 001–009.
Danso, D., Chow, J., Streit, W.R., 2019. Plastics: environmental and biotechnological perspectives on microbial degradation. Appl. Environ. Microbiol 85.
Danso, D., Schmeisser, C., Chow, J., Zimmermann, W., Wei, R., Leggewie, C., Li, X., Hazen, T., Streit, W.R., 2018. New insights into the function and global distribution of polyethylene terephthalate (PET)-degrading bacteria and enzymes in marine and terrestrial metagenomes. Appl. Environ. Microbiol 84.
Dodman, R., Reinke, J., 1982. A selective medium for determining the population of viable conidia of *Cochliobolus sativus* in soil. Aust. J. Agric. Res. 33, 287–293.
Donaghy, J., Kelly, P.F., McKay, A.M., 1998. Detection of ferulic acid esterase production by Bacillus spp. and lactobacilli. Appl. Microbiol. Biotechnol. 50, 257–260.
Dong, M., Zhang, Q., Xing, X., Chen, W., She, Z., Luo, Z., 2020. Raman spectra and surface changes of microplastics weathered under natural environments. Sci. Total Environ. 739, 139990.
Eastoe, J.E., 1955. The amino acid composition of mammalian collagen and gelatin. Biochem. J. 61, 589–600.
Eastoe, J.E., 1957. The amino acid composition of fish collagen and gelatin. Biochem. J. 65, 363–368.
Eddy, S.R., 2011. Accelerated Profile HMM Searches. PLoS Comput. Biol. 7, e1002195.
Edelmann, S., Staben, C., 1994. A statistical analysis of sequence geatures within genes from neurospora crassa. Exp. Mycol. 18, 70–81.
Ene, I.V., Bennett, R.J., Anderson, M.Z., 2019. Mechanisms of genome evolution in Candida albicans. Curr. Opin. Microbiol. 52, 47–54.
Fernández-Sanmartín, P., Requena Menéndez, A., Martínez Cortizas, A., A, E., 2023. Chemical characterisation of the mycodegradation of plastic using FTIR-ATR. Front. Microbiol.
Gaur, N., Narasimhulu, K., Pydi Setty, Y., 2018. Extraction of ligninolytic enzymes from novel Klebsiella pneumoniae strains and its application in wastewater treatment. Appl. Water Sci. 8, 111.
Gaytan, I., Sanchez-Reyes, A., Burelo, M., Vargas-Suarez, M., Liachko, I., Press, M., Sullivan, S., Cruz-Gomez, M.J., Loza-Tavera, H., 2019. Degradation of recalcitrant polyurethane and xenobiotic additives by a selected landfill microbial community and its biodegradative potential revealed by proximity ligation-based metagenomic analysis. Front. Microbiol. 10, 2986.
Geyer, R., 2020. Chapter 2 - Production, use, and fate of synthetic polymers. In: Letcher, T.M. (Ed.), Plastic Waste and Recycling. Academic Press, pp. 13–32.
Geyer, R., Jambeck, J.R., Law, K.L., 2017. Production, use, and fate of all plastics ever made. Sci. Adv. 3, e1700782.
Gomez, M., Reggio, D., Lazzari, M., 2019. Detection of degradation markers from polymer surfaces by a novel SERS-based strategy. Talanta 191, 156–161.
Gostinčar, C., Stajich, J.E., Zupancic, J., Zalar, P., Gunde-Cimerman, N., 2018. Genomic evidence for intraspecific hybridization in a clonal and extremely halotolerant yeast. BMC Genom. 19, 364.
Grabherr, M.G., Haas, B.J., Yassour, M., Levin, J.Z., Thompson, D.A., Amit, I., Adiconis, X., Fan, L., Raychowdhury, R., Zeng, Q., et al., 2011. Full-length transcriptome assembly from RNA-Seq data without a reference genome. Nat. Biotechnol. 29, 644–652.
Grigoriev, I.V., Nordberg, H., Shabalov, I., Aerts, A., Cantor, M., Goodstein, D., Kuo, A., Minovitsky, S., Nikitin, R., Ohm, R.A., et al., 2012. The genome portal of the Department of Energy Joint Genome Institute. Nucleic Acids Res. 40, D26–D32.
Guido Van, R., Fred, L.D., 2009. Python 3 Reference Manual %@ 1441412697. CreateSpace.
Guo, X., Lin, Z., Wang, Y., He, Z., Wang, M., Jin, G., 2019. In-line monitoring the degradation of polypropylene under multiple extrusions based on Raman spectroscopy. Polymers 11.
Hankin, L., Anagnostakis, S.L., 1975. The Use Of Solid Media For Detection Of Enzyme Production By Fungi. Mycologia 67, 597–607.
Hankin, L., Zucker, M., Sands, D.C., 1971. Improved solid medium for the detection and enumeration of pectolytic bacteria. Appl. Microbiol 22, 205–209.
Harwood, C.R., Cutting, S.M., 1990. Appendix 1—Media. Molecular Biological Methods for Bacillus. Wiley, Chichester, UK; New York, NY, USA.
Hassan Sel, D., Bell, T.H., Stefani, F.O., Denis, D., Hijri, M., St-Arnaud, M., 2014. Contrasting the community structure of arbuscular mycorrhizal fungi from hydrocarbon-contaminated and uncontaminated soils following willow (Salix spp. L.) planting. PLoS One 9, e102838.
Hitha, P.K., Girija, D., 2014. Isolation and screening of native microbial isolates for pectinase activity. Int. J. Sci. Res. 3, 632–634.
Huarte-Bonnet, C., Juarez, M.P., Pedrini, N., 2015. Oxidative stress in entomopathogenic fungi grown on insect-like hydrocarbons. Curr. Genet. 61, 289–297.
Hunter, J.D., 2007. Matplotlib: a 2D graphics environment. Comput. Sci. Eng. 9, 90–95.
Jeon, H.J., Kim, M.N., 2016. Isolation of mesophilic bacterium for biodegradation of polypropylene. Int. Biodeterior. Biodegrad. 115, 244–249.
Jimenez, D.J., Hector, R.E., Riley, R., Lipzen, A., Kuo, R.C., Amirebrahimi, M., Barry, K. W., Grigoriev, I.V., van Elsas, J.D., Nichols, N.N., 2017. Draft genome sequence of coniochaeta ligniaria NRRL 30616, a lignocellulolytic fungus for bioabatement of inhibitors in plant biomass hydrolysates. Genome Announc 5.
Jones, J.G., Knight, M., Byrom, J.A., 1970. Effect of gross pollution by kerosine hydrocarbons on the Microflora of a moorland soil. Nature 227, 1166.
Joshi, N.A., and Fass, J.N. (2011). Sickle: A sliding-window, adaptice, quality-based trimming tool for FastQ files (https://github.com/najoshi/sickle).
Kamali, M., Khodaparast, Z., 2015. Review on recent developments on pulp and paper mill wastewater treatment. Ecotoxicol. Environ. Saf. 114, 326–342.
Kang, C.H., Oh, K.H., Lee, M.H., Oh, T.K., Kim, B.H., Yoon, J., 2011. A novel family VII esterase with industrial potential from compost metagenomic library. Micro Cell Fact. 10, 41.
Kaushal, J., Khatri, M., Arya, S.K., 2021. Recent insight into enzymatic degradation of plastics prevalent in the environment: A mini - review. Clean. Eng. Technol. 2.
Kriventseva, E.V., Kuznetsov, D., Tegenfeldt, F., Manni, M., Dias, R., Simao, F.A., Zdobnov, E.M., 2019. OrthoDB v10: sampling the diversity of animal, plant, fungal, protist, bacterial and viral genomes for evolutionary and functional annotations of orthologs. Nucleic Acids Res 47, D807–D811.
Kurtzman, C.P., Robnett, C.J., 1997. Identification of clinically important ascomycetous yeasts based on nucleotide divergence in the 5′ end of the large-subunit (26S) ribosomal DNA gene. J. Clin. Microbiol. 35, 1216–1223.
LaBella, A.L., Opulente, D.A., Steenwyk, J.L., Hittinger, C.T., Rokas, A., 2019. Variation and selection on codon usage bias across an entire subphylum. PLoS Genet 15, e1008304.
Lauer, B.H., Baker, B.E., 1977. Amino acid composition of casein isolated from the milks of different species. Can. J. Zool. 55, 231–236.
Lawrence, D.P., Nouri, M.T., Trouillas, F.P., 2021. Pleurostoma decline of olive trees caused by pleurostoma richardsiae in California. Plant Dis. 105, 2149–2159.
Leahy, J.G., Colwell, R.R., 1990. Microbial degradation of hydrocarbons in the environment. Microbiol Rev. 54, 305–315.
Lelliott, R.A., Stead, D.E., 1987. Methods for the Diagnosis of Bacterial Diseases of Plants. Blackwell, Oxford.
Leonhardt, S., Buttner, E., Gebauer, A.M., Hofrichter, M., Kellner, H., 2018. Draft Genome Sequence of the Sordariomycete Lecythophora (Coniochaeta) hoffmannii CBS 245.38. Genome Announc 6, e01510–e01517.
Levenstadt, J.S., Poutanen, S.M., Mohan, S., Zhang, S., Silverman, M., 2012. Pleurostomophora richardsiae - an insidious fungus presenting in a man 44 years after initial inoculation: a case report and review of the literature. Can. J. Infect. Dis. Med Microbiol 23, 110–113.
Leveson-Gower, R.B., Mayer, C., Roelfes, G., 2019. The importance of catalytic promiscuity for enzyme design and evolution. Nat. Rev. Chem. 3, 687–705.
Lloyd, A.T., Sharp, P.M., 1991. Codon usage in Aspergillus nidulans. Mol. Gen. Genet. 230, 288–294.
Lowe, R.G., Howlett, B.J., 2012. Indifferent, affectionate, or deceitful: lifestyles and secretomes of fungi. PLoS Pathog. 8, e1002515.
Manni, M., Berkeley, M.R., Seppey, M., Simao, F.A., Zdobnov, E.M., 2021. BUSCO update: novel and streamlined workflows along with broader and deeper phylogenetic coverage for scoring of eukaryotic, prokaryotic, and viral genomes. Mol. Biol. Evol. 38, 4647–4654.
Marriott, D.J., Wong, K.H., Aznar, E., Harkness, J.L., Cooper, D.A., Muir, D., 1997. Scytalidium dimidiatum and Lecythophora hoffmannii: unusual causes of fungal infections in a patient with AIDS. J. Clin. Microbiol. 35, 2949–2952.
Mayumi, D., Akutsu-Shigeno, Y., Uchiyama, H., Nomura, N., Nakajima-Kambe, T., 2008. Identification and characterization of novel poly(DL-lactic acid) depolymerases from metagenome. Appl. Microbiol. Biotechnol. 79, 743–750.
Mei, T., Wang, J., Xiao, X., Lv, J., Li, Q., Dai, H., Liu, X., Pi, F., 2022. Identification and Evaluation of Microplastics from Tea Filter Bags Based on Raman Imaging. Foods 11, 2871.
Mondo, S.J., Jimenez, D.J., Hector, R.E., Lipzen, A., Yan, M., LaButti, K., Barry, K., van Elsas, J.D., Grigoriev, I.V., Nichols, N.N., 2019. Genome expansion by

allopolyploidization in the fungal strain Coniochaeta 2T2.1 and its exceptional lignocellulolytic machinery. Biotechnol. Biofuels 12, 229.
Muller, C.A., Perz, V., Provasnek, C., Quartinello, F., Guebitz, G.M., Berg, G., 2017. Discovery of Polyesterases from Moss-Associated Microorganisms. Appl. Environ. Microbiol 83.
Naranjo-Ortiz, M.A., Gabaldon, T., 2019. Fungal evolution: diversity, taxonomy and phylogeny of the Fungi. Biol. Rev. Camb. Philos. Soc. 94, 2101–2137.
Nelson, A.R., Narrowe, A.B., Rhoades, C.C., Fegel, T.S., Daly, R.A., Roth, H.K., Chu, R.K., Amundson, K.K., Young, R.B., Steindorff, A.S., et al., 2022. Wildfire-dependent changes in soil microbiome diversity and function. Nat. Microbiol 7, 1419–1430.
Nelson, D.R., 2018. Cytochrome P450 diversity in the tree of life. Biochim. Biophys. Acta Proteins Prote 1866, 141–154.
Nordberg, H., Cantor, M., Dusheyko, S., Hua, S., Poliakov, A., Shabalov, I., Smirnova, T., Grigoriev, I.V., Dubchak, I., 2014. The genome portal of the Department of Energy Joint Genome Institute: 2014 updates. Nucleic Acids Res 42, D26–D31.
Ojha, N., Pradhan, N., Singh, S., Barla, A., Shrivastava, A., Khatua, P., Rai, V., Bose, S., 2017. Evaluation of HDPE and LDPE degradation by fungus, implemented by statistical optimization. Sci. Rep. 7, 39515.
Oliya, P., Singh, S., Goel, N., Sing, U.P., Srivastava, A.K., 2020. Polypropylene degradation potential of microbes isolated from solid waste dumping site. Pollut. Res 39, 268–277.
Pallister, E., Gray, C.J., Flitsch, S.L., 2020. Enzyme promiscuity of carbohydrate active enzymes and their applications in biocatalysis. Curr. Opin. Struct. Biol. 65, 184–192.
Paterson, R.R.M., Bridge, P.D., 1994. Biochemical Techniques for Filamentous Fungi. CAB International, Wallingford, UK.
Peden, J.F., 1999. Analysis of Codon Usage. Department of Genetics (University of Nottingham), p. 226.
Pedregosa, F., Varoquaux, G., Gramfort, A., Michel, V., Thirion, B., 2011. Scikit-learn: machine learning in python. J. Mach. Learn. Res. 12, 2825–2830.
Peixoto, J., Silva, L.P., Kruger, R.H., 2017. Brazilian Cerrado soil reveals an untapped microbial potential for unpretreated polyethylene biodegradation. J. Hazard Mater. 324, 634–644.
Phan, S., Padilla-Gamiño, J.L., Luscombe, C.K., 2022. The effect of weathering environments on microplastic chemical identification with Raman and IR spectroscopy: Part I. polyethylene and polypropylene. Polym. Test. 116.
Pinnell, L.J., Turner, J.W., 2019. Shotgun metagenomics reveals the benthic microbial community response to plastic and bioplastic in a coastal marine environment. Front. Microbiol. 10, 1252.
Popovic, A., Hai, T., Tchigvintsev, A., Hajighasemi, M., Nocek, B., Khusnutdinova, A.N., Brown, G., Glinos, J., Flick, R., Skarina, T., et al., 2017. Activity screening of environmental metagenomic libraries reveals novel carboxylesterase families. Sci. Rep. 7, 44103.
Prjibelski, A., Antipov, D., Meleshko, D., Lapidus, A., Korobeynikov, A., 2020. Using SPAdes De Novo Assembler. Curr. Protoc. Bioinforma. 70, e102.
Puspitasari, N., Tsai, S.L., Lee, C.K., 2021. Fungal hydrophobin RolA enhanced PETase hydrolysis of polyethylene terephthalate. Appl. Biochem. Biotechnol. 193, 1284–1295.
R Development Core Team, 2020. R: A Languange and Environment for Statistical Computing. R Foundation for Statistical Computing, (Vienna, Austria.
Rana, A.K., Thakur, M.K., Saini, A.K., Mokhta, S.K., Moradi, O., Rydzkowski, T., Alsanie, W.F., Wang, Q., Grammatikos, S., Thakur, V.K., 2022. Recent developments in microbial degradation of polypropylene: Integrated approaches towards a sustainable environment. Sci. Total Environ. 826, 154056.
Rice, P., Longden, I., Bleasby, A., 2000. EMBOSS: the European Molecular Biology Open Software Suite. Trends Genet 16, 276–277.
Russell, J.R., Huang, J., Anand, P., Kucera, K., Sandoval, A.G., Dantzler, K.W., Hickman, D., Jee, J., Kimovec, F.M., Koppstein, D., et al., 2011. Biodegradation of polyester polyurethane by endophytic fungi. Appl. Environ. Microbiol 77, 6076–6084.
Ryberg, M.W., Laurent, A., Hauschild, M., 2018. Mapping of global plastics value chain and plastics losses to the environment (with a particular focus on marine environment). Paper presented at: UN Environment. UNESCO,, Nairobi, Kenya.
Sankara Subramanian, S.H., Balachandran, K.R.S., Rangamaran, V.R., Gopal, D., 2020. RemeDB: tool for rapid prediction of enzymes involved in bioremediation from high-throughput metagenome data sets. J. Comput. Biol. 27, 1020–1029.
Satow, M.M., Attili-Angelis, D., de Hoog, G.S., Angelis, D.F., Vicente, V.A., 2008. Selective factors involved in oil flotation isolation of black yeasts from the environment. Stud. Mycol. 61, 157–163.
Schindelin, J., Arganda-Carreras, I., Frise, E., Kaynig, V., Longair, M., Pietzsch, T., Preibisch, S., Rueden, C., Saalfeld, S., Schmid, B., et al., 2012. Fiji: an open-source platform for biological-image analysis. Nat. Methods 9, 676–682.
Sharp, P.M., Li, W.H., 1987. The codon Adaptation Index–a measure of directional synonymous codon usage bias, and its potential applications. Nucleic Acids Res. 15, 1281–1295.
Sheik, S., Chandrashekar, K.R., Swaroop, K., Somashekarappa, H.M., 2015. Biodegradation of gamma irradiated low density polyethylene and polypropylene by endophytic fungi. Int. Biodeterior. Biodegrad. 105, 21–29.
Sievers, F., Wilm, A., Dineen, D., Gibson, T.J., Karplus, K., Li, W., Lopez, R., McWilliam, H., Remmert, M., Soding, J., et al., 2011. Fast, scalable generation of high-quality protein multiple sequence alignments using Clustal Omega. Mol. Syst. Biol. 7, 539.
Sista Kameshwar, A.K., Qin, W., 2018. Comparative study of genome-wide plant biomass-degrading CAZymes in white rot, brown rot and soft rot fungi. Mycology 9, 93–105.
Smit, A.F.A., Hubley, R., and Green, P. (2013–2015). RepeatMasker (⟨http://www.repeatmasker.org⟩).
Stanke, M., Morgenstern, B., 2005. AUGUSTUS: a web server for gene prediction in eukaryotes that allows user-defined constraints. Nucleic Acids Res 33, W465–W467.
Sulaiman, S., Yamato, S., Kanaya, E., Kim, J.J., Koga, Y., Takano, K., Kanaya, S., 2012. Isolation of a novel cutinase homolog with polyethylene terephthalate-degrading activity from leaf-branch compost by using a metagenomic approach. Appl. Environ. Microbiol 78, 1556–1562.
Tchigvintsev, A., Tran, H., Popovic, A., Kovacic, F., Brown, G., Flick, R., Hajighasemi, M., Egorova, O., Somody, J.C., Tchigvintsev, D., et al., 2015. The environment shapes microbial enzymes: five cold-active and salt-resistant carboxylesterases from marine metagenomes. Appl. Microbiol Biotechnol. 99, 2165–2178.
Teramoto, H., Tanaka, H., Wariishi, H., 2004. Degradation of 4-nitrophenol by the lignin-degrading basidiomycete Phanerochaete chrysosporium. Appl. Microbiol Biotechnol. 66, 312–317.
Tournier, V., Topham, C.M., Gilles, A., David, B., Folgoas, C., Moya-Leclair, E., Kamionka, E., Desrousseaux, M.L., Texier, H., Gavalda, S., et al., 2020. An engineered PET depolymerase to break down and recycle plastic bottles. Nature 580, 216–219.
Underlin, E.N., Frommhagen, M., Dilokpimol, A., van Erven, G., de Vries, R.P., Kabel, M. A., 2020. Feruloyl Esterases for Biorefineries: Subfamily Classified Specificity for Natural Substrates. Front Bioeng. Biotechnol. 8, 332.
Van Den Ende, A., De Hoog, G., 1999. Variability and molecular diagnostics of the neurotropic species Cladophialophora bantiana. Stud. Mycol. 43, 151–162.
Virtanen, P., Gommers, R., Oliphant, T.E., Haberland, M., Reddy, T., Cournapeau, D., Burovski, E., Peterson, P., Weckesser, W., Bright, J., et al., 2020. SciPy 1.0: fundamental algorithms for scientific computing in Python. Nat. Methods 17, 261–272.
Waring, R.H., Harris, R.M., Mitchell, S.C., 2018. Plastic contamination of the food chain: A threat to human health? Maturitas 115, 64–68.
Waskom, M., 2021. seaborn: statistical data visualization. J. Open Source Softw. 6.
Webb, J.S., Nixon, M., Eastwood, I.M., Greenhalgh, M., Robson, G.D., Handley, P.S., 2000. Fungal colonization and biodeterioration of plasticized polyvinyl chloride. Appl. Environ. Microbiol. 66, 3194–3200.
Weber, E., 2002. The lecythophora-coniochaeta complex: I. Morphological studies on Lecythophora species isolated from Picea abies. Nova Hedwig. 74, 159–185.
Wessels, J., De Vries, O., Asgeirsdottir, S.A., Schuren, F., 1991. Hydrophobin genes involved in formation of aerial hyphae and fruit bodies in schizophyllum. Plant Cell 3, 793–799.
White, T.J., Bruns, T.D., Lee, S.B., Taylor, J.W., 1990. Amplification and Direct Sequencing of Fungal Ribosomal RNA Genes for Phylogenetics. In: Innis, M.A., Gelfand, D.H., Sninsky, J.J., White, T.J. (Eds.), PCR Protocols: A Guide to Methods and Applications. Academic Press, New York, pp. 315–322.
Wilken, S.E., Seppala, S., Lankiewicz, T.S., Saxena, M., Henske, J.K., Salamov, A.A., Grigoriev, I.V., O'Malley, M.A., 2020. Genomic and proteomic biases inform metabolic engineering strategies for anaerobic fungi. Metab. Eng. Commun. 10, e00107.
Wood, V., Gwilliam, R., Rajandream, M.A., Lyne, M., Lyne, R., Stewart, A., Sgouros, J., Peat, N., Hayles, J., Baker, S., et al., 2002. The genome sequence of Schizosaccharomyces pombe. Nature 415, 871–880.
Yang, S.S., Ding, M.Q., He, L., Zhang, C.H., Li, Q.X., Xing, D.F., Cao, G.L., Zhao, L., Ding, J., Ren, N.Q., et al., 2021. Biodegradation of polypropylene by yellow mealworms (Tenebrio molitor) and superworms (Zophobas atratus) via gut-microbe-dependent depolymerization. Sci. Total Environ. 756, 144087.
Yee, M.S., Hii, L.W., Looi, C.K., Lim, W.M., Wong, S.F., Kok, Y.Y., Tan, B.K., Wong, C.Y., Leong, C.O., 2021. Impact of Microplastics and Nanoplastics on Human Health. Nanomater. (Basel) 11, 496.
Zajc, J., Gostincar, C., Cernosa, A., Gunde-Cimerman, N., 2019. Stress-tolerant yeasts: opportunistic pathogenicity versus biocontrol potential. Genes 10, 42.
Zdobnov, E.M., Kuznetsov, D., Tegenfeldt, F., Manni, M., Berkeley, M., Kriventseva, E.V., 2021. OrthoDB in 2020: evolutionary and functional annotations of orthologs. Nucleic Acids Res. 49, D389–D393.
Zhang, H., Yohe, T., Huang, L., Entwistle, S., Wu, P., Yang, Z., Busk, P.K., Xu, Y., Yin, Y., 2018. dbCAN2: a meta server for automated carbohydrate-active enzyme annotation. Nucleic Acids Res. 46, W95–W101.
Zhou, Z., Dang, Y., Zhou, M., Li, L., Yu, C.H., Fu, J., Chen, S., Liu, Y., 2016. Codon usage is an important determinant of gene expression levels largely through its effects on transcription. Proc. Natl. Acad. Sci. USA 113, E6117–E6125.
Zhu, B., Wang, D., Wei, N., 2022. Enzyme discovery and engineering for sustainable plastic recycling. Trends Biotechnol. 40, 22–37.